# CERIUM MODIFIED NICKEL AND IRON BASED OXYGEN CARRIERS FOR CHEMICAL LOOPING COMBUSTION

BY

Shamseldin Awad Hagahmed Mohamed

A Thesis Presented to the

DEANSHIP OF GRADUATE STUDIES

**KING FAHD UNIVERSITY OF PETROLEUM & MINERALS**

DHAHRAN, SAUDI ARABIA

In Partial Fulfillment of the
Requirements for the Degree of

# MASTER OF SCIENCE

In

**CHEMICAL ENGINEERING**

**October 2014**

KING FAHD UNIVERSITY OF PETROLEUM & MINERALS

DHAHRAN- 31261, SAUDI ARABIA

**DEANSHIP OF GRADUATE STUDIES**

This thesis, written by **Shamseldin Awad Hagahmed Mohamed** under the direction of his thesis advisor and approved by his thesis committee, has been presented and accepted by the Dean of Graduate Studies, in partial fulfillment of the requirements for the degree of **MASTER OF SCIENCE IN CHEMICAL ENGINEERING**

Shaikh Abdur Razzak

Dr. Abdur Razzak Shaikh
(Advisor)

Dr. Mohammed Ba-Shammakh
Department Chairman

Mozahar Hossain

Dr. M. Mozahar Hossain
(Co-Advisor)

Dr. Salam A. Zummo
Dean of Graduate Studies

Dr. Mohammed Ba-Shammakh
(Member)

21/9/14

Date


Dr. Abdallah Al-Shammari
(Member)

Dr. Eid Musaad Al-Mutairi
(Member)

*To my mother, for everything*

*To Awadallah, Shaima, Abulgasim, Ibrahim and Sara,*
*for the love and support*

*In memory of*

*My father*

*My friend Ahmed Hassan*

# ACKNOWLEDGMENTS

I would like to convey my gratitude to everyone who made it possible to accomplish this work. Many thanks go to my Thesis advisor Dr. Shaikh Abdur Razzak and my co-advisor Dr. M. Mozahar Hossain for their endless patience, support and encouragement. I would like also to thank my Thesis committee members: Dr. Mohammed Ba-Shammakh, Dr. Abdallah A. Al-Shammari and Dr. Eid M. Al-Mutairi for their valuable comments.

I am very grateful to King Fahd University of Petroleum and Minerals for giving me the opportunity to pursue my graduate study, and to the Chemical Engineering Department. I thank all my colleagues and friends at King Fahd University of Petroleum and Minerals for making it such a wonderful time and experience.

I would like to acknowledge the support provided by King Abdulaziz City for Science and Technology (KACST) through the Science & Technology Unit at King Fahd University of Petroleum & Minerals (KFUPM) for funding this work through project No. 11-ENV1655-04 as a part of the National Science, Technology and Innovation Plan.

Finally, I would like to express my sincere gratitude to my mother and my family members for the love and support. Also many thanks go to my roommate and friend Mohanned and all my friends from Chemical Engineering Department of Khartoum University.

# TABLE OF CONTENTS

**ACKNOWLEDGMENTS** ..... **V**

**TABLE OF CONTENTS** ..... **VI**

**LIST OF TABLES** ..... **VIII**

**LIST OF FIGURES** ..... **IX**

**ABSTRACT** ..... **XI**

**CHAPTER 1 INTRODUCTION** ..... **1**

**CHAPTER 2 LITERATURE REVIEW** ..... **8**

2.1 CARBON DIOXIDE CAPTURE TECHNIQUES ..... 8

2.1.1 POST COMBUSTION ..... 8

2.1.2 PRE-COMBUSTION ..... 9

2.1.3 OXY-FUEL COMBUSTION ..... 10

2.2 CHEMICAL LOOPING COMBUSTION ..... 12

2.2.1 OXYGEN CARRIERS ..... 15

2.2.2 CHEMISTRY ..... 20

2.2.3 REACTION KINETICS ..... 22

**CHAPTER 3 OBJECTIVES** ..... **26**

**CHAPTER 4 EXPERIMENTAL AND METHODOLOGY** ..... **27**

4.1 OXYGEN CARRIER PREPARATION ..... 27

4.2 TEMPERATURE PROGRAMMED STUDIES ..... 30

4.2.1 TPR/TPO EXPERIMENTS ..... 30

4.2.2 PULSE CHEMISORPTION ..... 31

4.3 CREC RISER SIMULATOR ..... 32

4.4 NITROGEN ADSORPTION AND XRD ..... 34

**CHAPTER 5 RESULTS AND DISCUSSION** ..... **35**

5.1 TEMPERATURE PROGRAMMED STUDIES ..... 36

5.1.1 IRON BASED OXYGEN CARRIERS ..... 36
5.1.2 NI BASED OXYGEN CARRIERS ..... 39
5.2 OXYGEN CARRIER CHARACTERIZATION ..... 45
5.3 X-RAY DIFFRACTION TEST ..... 50
5.4 SOLID STATE REDUCTION KINETICS ..... 51
5.5 CREC RISER SIMULATOR REACTIVITY STUDIES ..... 55
5.5.1 IRON BASED OXYGEN CARRIERS ..... 56
5.5.2 NI BASED OXYGEN CARRIERS ..... 58
**CHAPTER 6 CONCLUSION AND RECOMMENDATIONS ..... 66**
6.1 CONCLUSION ..... 66
6.2 RECOMMENDATIONS ..... 67
**REFERENCES ..... 69**
**VITAE ..... 76**

# LIST OF TABLES

Table 1: List of prepared oxygen carrier samples ..... 35
Table 2: $N_2$ adsorption results ..... 46
Table 3: Dispersion and crystal size results ..... 49
Table 4: Activation energy for the reduction of nickel oxide ..... 55

# LIST OF FIGURES

Figure 1: Global surface temperature of the earth, Source (NASA satellite observations) 1
Figure 2: Worldwide Greenhouse gases emissions, Source (IPCC, 2014) ..... 2
Figure 3: Global greenhouse gases emissions by gas, Source (IPCC, 2007) ..... 3
Figure 4: Carbon dioxide emissions by source ..... 4
Figure 5: Energy sources by fuel type ..... 6
Figure 6: $CO_2$ capture techniques ..... 10
Figure 7: Schematic description of chemical-looping combustion process ..... 12
Figure 8: Simplified chemical looping combustion process flow diagram, Source (Moghtaderi, 2011) ..... 14
Figure 9: Reaction models in the particle: a) Changing grain size model (CGSM); b) Shrinking core model (SCM), Source (Hossain and de Lasa, 2008) ..... 23
Figure 10: Nucleation growth model, Source (Hossain and de Lasa, 2008) ..... 23
Figure 11: Incipient wetness technique ..... 28
Figure 12: Thermal treatment process illustration ..... 29
Figure 13: Schematic diagram of AutoChem II ..... 31
Figure 14: CREC simulator Schematic Diagram, Source (Hossain and de Lasa, 2008) .. 32
Figure 15: TPR profiles of (i) $Fe_2O_3$(20)/Ce(1)-$\gamma Al_2O_3$ (ii) $Fe_2O_3$(15)/Ce(1)-$\gamma Al_2O_3$ sampels ..... 37
Figure 16: Reduction percentage of $Fe_2O_3$(15)/Ce(1)-$\gamma Al_2O_3$ under repeated cycles ..... 38
Figure 17: Reduction percentage of $Fe_2O_3$(20)/Ce(1)-$\gamma Al_2O_3$ under repeated cycles ..... 39
Figure 18: TPR profiles of (i) $\gamma Al_2O_3$ (ii) NiO/$\gamma Al_2O_3$ and (iii) NiO/Ce-$\gamma Al_2O_3$ samples 39
Figure 19: ((TPR profiles of (i)NiO/Ce(1)-$\gamma Al_2O_3$ (ii) NiO/Ce(5)-$\gamma Al_2O_3$ sampels ..... 41
Figure 20: Effect of Ce modification on percent of nickel oxide reduction ..... 43
Figure 21: Percent of nickel oxide reduction of NiO/Ce(1)-$\gamma Al_2O_3$ sample over repeated TPR/TPO cycles ..... 45
Figure 22: $N_2$ adsorption isotherms ..... 46
Figure 23: Pulse chemisorption profile ..... 47
Figure 24: SEM mapping for NiO/Ce(1)-$\gamma Al_2O_3$ (left) nd NiO/Ce(5)-$\gamma Al_2O_3$ (right) ..... 49
Figure 25: XRD Patterns of the prepared oxygen carriers ..... 50

Figure 26: Experimental versus model predicted conversion of nickel oxide (alpha) using NiO/Ce(1)-$\gamma Al_2O_3$ oxygen carrier ..... 54
Figure 27: Experimental versus model predicted conversion of nickel oxide (alpha) using NiO/Ce(5)-$\gamma Al_2O_3$ oxygen carrier ..... 54
Figure 28: Pressure profile during the combustion process for $Fe_2O_3$(20)/Ce(1)-$\gamma Al_2O_3$ 56
Figure 29: Ethane conversion during multiple cycles in CREC Simulator ..... 57
Figure 30: Iron conversion during multiple cycles in CREC Simulator ..... 57
Figure 31: Pressure profile during the combustion process for NiO/Ce(1)-$\gamma Al_2O_3$ ..... 60
Figure 32: Methane conversion for modified and un-modified oxygen carrier over multiple CLC cycles ..... 63
Figure 33: NiO conversion for modified and un-modified oxygen carrier over multiple CLC cycles ..... 63
Figure 34: Effect of reaction temperature on NiO conversion ..... 64
Figure 35: Effect of reaction time on NiO conversion ..... 65

# ABSTRACT

Full Name : Shamseldin Awad Hagahmed Mohamed

Thesis Title : Cerium Modified Nickel And Iron Based Oxygen Carriers For Chemical Looping Combustion

Major Field : Chemical Engineering

Date of Degree : September 2014

The present Thesis reports the promotional effects of Ce modification on a NiO/Ce-$\gamma Al_2O_3$ and $Fe_2O_3$/Ce-$\gamma Al_2O_3$ oxygen carriers for chemical-looping combustion (CLC). The oxygen carrier samples were prepared by an incipient wetness technique using a successive metal loading. The reduction characteristics of the prepared oxygen carriers were evaluated in repeated temperature programmed reduction/oxidation cycles. The results show that the presence of Ce minimizes the metal support interaction and improves the reducibility and oxygen carrying capacity of the oxygen carriers. As a result, almost 94 % of the loaded nickel oxide species on Ce-$\gamma Al_2O_3$ have been reduced as opposed to only 70 % reduction of nickel oxide species on $\gamma Al_2O_3$. The presence of Ce also provides stable reduction performance over repeated oxidation/reduction cycles, which is essential for a CLC process. The sustained reducibility of the samples is mainly due to the absence of agglomeration and the formation of easily reducible nickel oxide species instead of nickel aluminate, as confirmed by the hydrogen pulse chemisorption and XRD analysis respectively. The EDX mapping of the oxygen carrier shows that the presence of Ce influences the uniform nickel dispersion on the support. A nucleation model was proposed to describe the solid-state reduction kinetics of the Ce modified NiO/Ce-$\gamma Al_2O_3$ oxygen carrier. The oxygen carriers were further evaluated in a fluidized

CREC Riser Simulator using methane/ethane as fuel and air for re-oxidation. The Ce containing oxygen carriers showed excellent reactivity and stability over the repeated fluidized CLC cycles.

# ملخص الرسالة

**الاسم الكامل: شمس الدين عوض حاج أحمد محمد**

**عنوان الرسالة: معالجة مركبات نقل الأكسجين مبنية على النيكل و الحديد بواسطة أكسيد السيريوم للاستخدام في عملية الاحتراق الكيميائي الحلقي**

**التخصص: هندسة كيميائية**

**تاريخ الدرجة العلمية: سبتمبر 2014**

هذه الأطروحة تدرس الآثار الإيجابية لإضافة Ce إلى $NiO/Ce-\gamma Al_2O_3$ المستخدم كناقل للأوكسجين في عمليات الاحتراق الكيميائي الحلقي. تم تحضير العينات باستخدام تقنية التحميل بواسطة التبلل مع تكرار عملية تحميل المعدن. أداء العينات لاتي تم تحضيرها في ما يتعلق بالأكسدة تم اختباره بواسطة تجارب اكسدة و اختزال متتالية TPR and TPO . تظهر النتائج أن وجود ال Ce يقلل من الترابط بين المعدن الفعال و الداعم و يحسن القدرة الاستيعابية للأوكسجين. نتيجة لذلك, ما يقرب من 94% من النيكل الموجود في العينة المعدلة بواسطة Ce تم اختزاله بالمقارنة مع 71% فقط للعينات غير المعدلة بواسطة Ce . تعديل العينات يؤثر ايضا على أداء ناقل الاوكسجين في المدى الطويل بحيث يوفر أداء مستقر في عمليات الاكسدة والاختزال المتتالية, وهو امر ضروري في عملية الاحتراق الكيميائي الحلقي التي هي في الاصل عمليات احتراق (اختزال) و اكسدة متتابعة. الأداء الممتاز للعينات المعدلة هو نتيجة لغياب التكتل في العينات كما هو واضح من نتائج اختبار pulse chemisorption, و تكون انواع سهلة الاختزال من أكاسيد النيكل بدلا من النيكل ألومينات, وهو ما أكدته اختبارات XRD. تم ايضا تحليل العينات بواسطة EDX وظهر أن اضافة Ce تساعد على تحميل النيكل على الداعم بصورة موحدة و مستمرة. تم تطوير نموذج رياضي لوصف حركية تفاعل الاختزال للعينات تحت البحث. تم حساب طاقة التفعيل و كانت 54 kJ/mole و النتيجة قريبة من القيم المنشورة في المراجع. أخيرا أختبرت العينات في مفاعل CREC Riser simulator باستخدام غازي الميثان والإيثان كوقود. العينات المعدلة أبدت خصائص تفاعلية ممتازة و استقرار خلال التفاعلات المتتالية.

# CHAPTER 1

# INTRODUCTION

In recent years the world became aware of the environmental impact of our human lifestyle; as environmental issues like global warming, climate change and greenhouse gases became a major concern to all the people around the globe.

It's evident that the earth is warming and since the late 19th century to the year 2012 the global average surface temperatures of the earth (land and ocean surface combined) have increased 0.85 ºC [1], not to mention that the linear trend for the last 50 years is about 0.13 $^{0}$C per decade which is double the increasing rate for the 100 years before (see Figure 1).

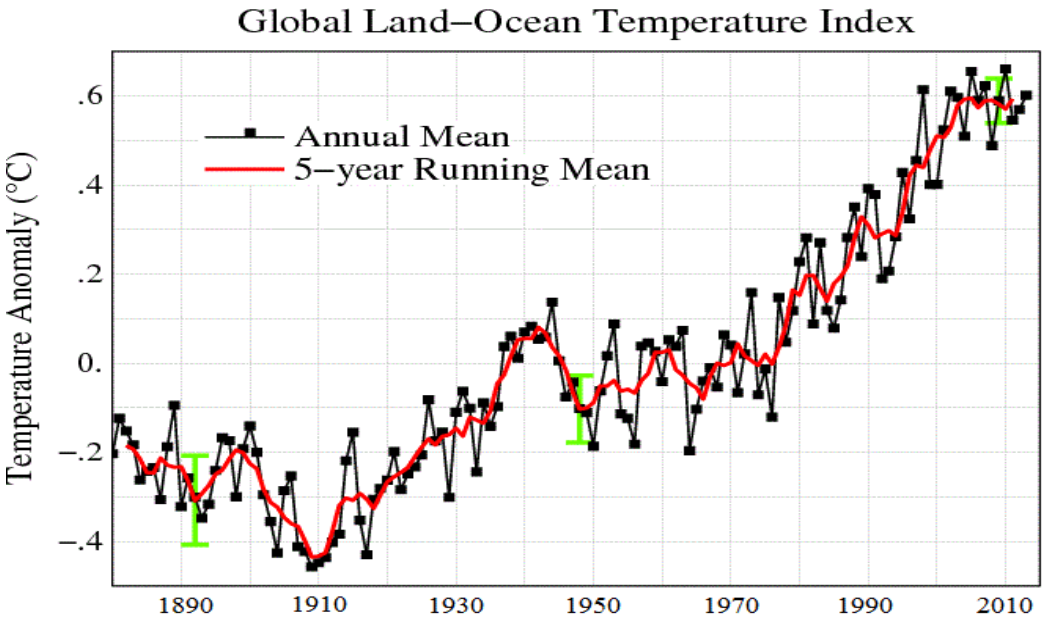


Figure 1: Global surface temperature of the earth, Source (NASA satellite observations)

This change can affect the biodiversity on the planet as well as the biological and physical systems.

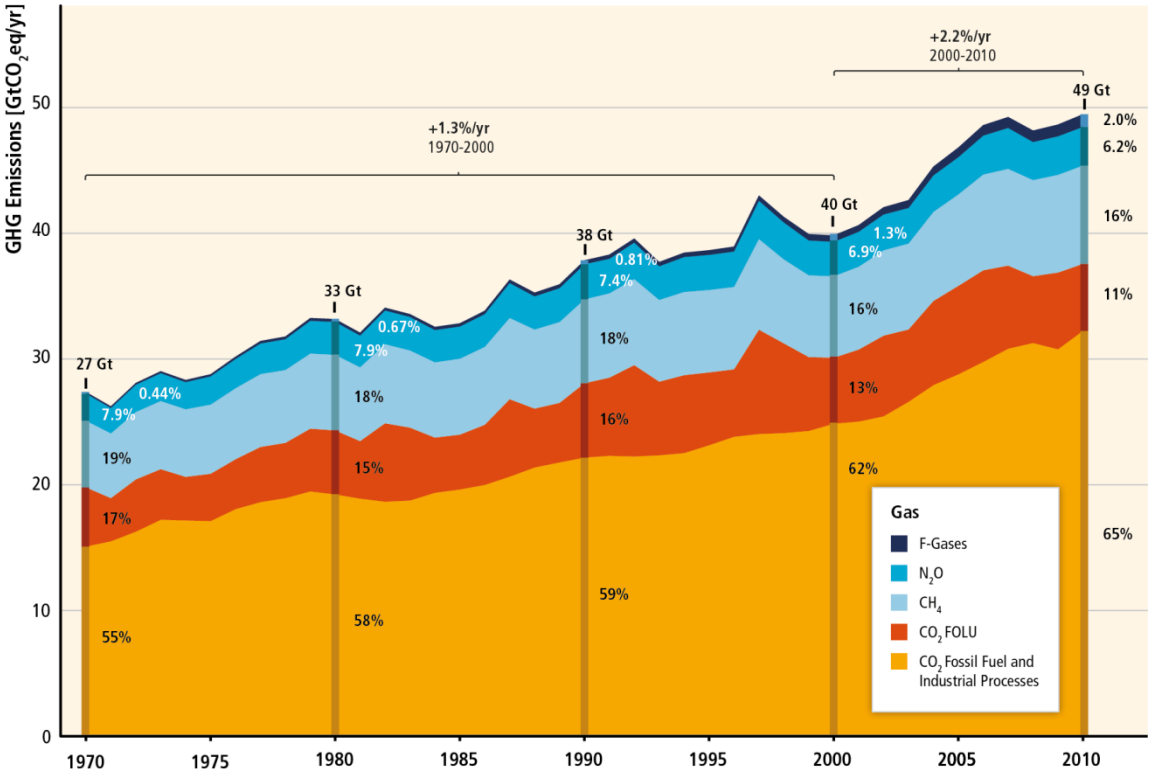


Figure 2: Worldwide Greenhouse gases emissions, Source (IPCC, 2014)

Majority of the scientists believe that the main cause behind the global warming is the increase of the anthropogenic greenhouse gases emissions such as carbon dioxide, methane, nitrogen oxides and hydro-fluorocarbons. These emissions have recorded a 70 % growth over the period between 1970 and 2004 according to IPCC [2]. Population growth, rapid urbanization and improving quality of human lifestyle are believed to be the major factors for greenhouse gases emissions.

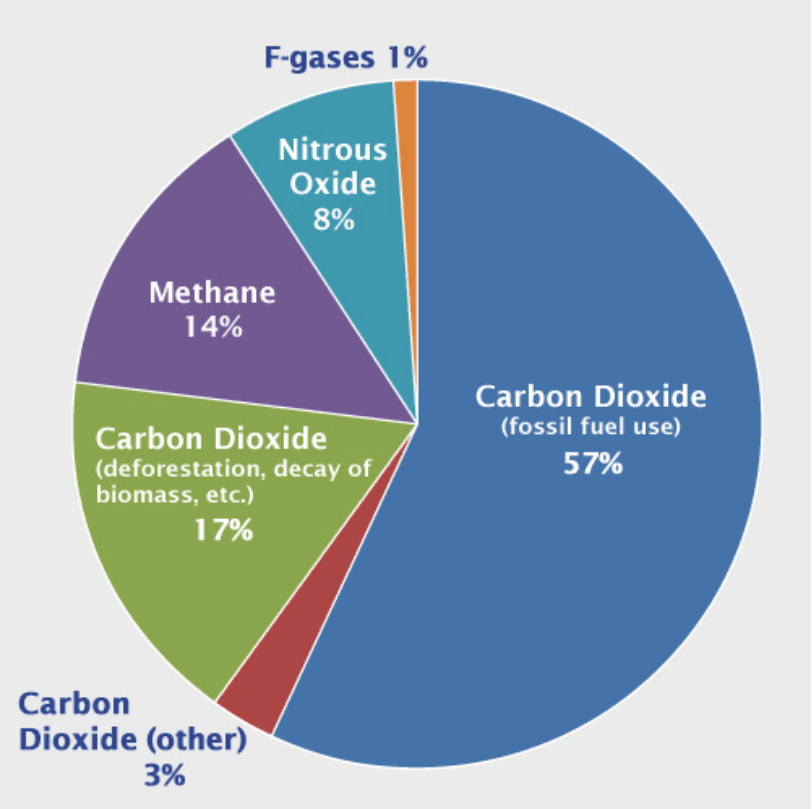


Figure 3: Global greenhouse gases emissions by gas, Source (IPCC, 2007)

The atmospheric concentrations of carbon dioxide exceeded the levels of the pre-industrial era by 40% to reach 391 ppm in 2011, and with a percentage of about 77% of the greenhouse gases emissions due to human activities in 2004 as presented in the figure above, carbon dioxide is considered the most significant anthropogenic greenhouse gas (GHG) when considering its emission control [1], [3].

The combustion of fossil based fuels to meet the world's energy demands coupled with industrial processes involving combustion of fossil based fuels are considered the main source of carbon dioxide emissions (Figure 4). Since the fossil based fuels are available and reliable their contribution is about 80 % of the energy supply worldwide [4]. All of

which had led to the increase of carbon dioxide global atmospheric concentration to 390 ppm in 2010 compared to 280 ppm in the pre-industrial era [5].

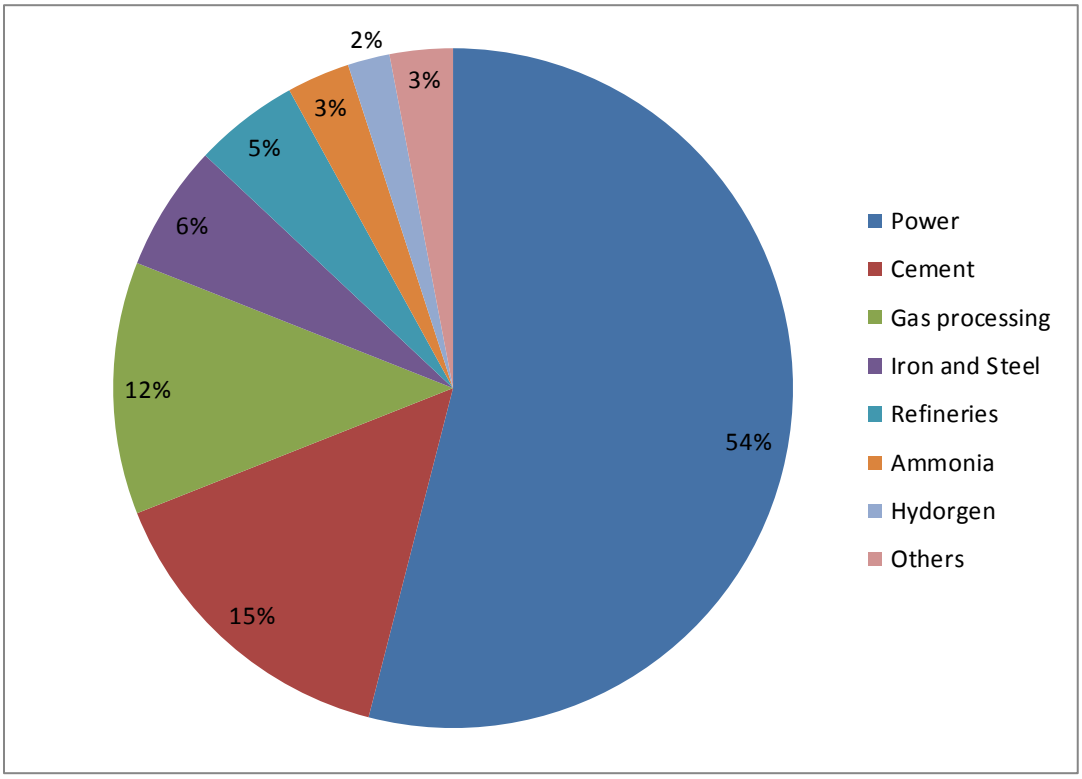


Figure 4: Carbon dioxide emissions by source

The combustion of fossil based fuels to meet the world's energy demands is considered the main source of carbon dioxide emissions representing about 57% of the world anthropogenic greenhouse gases emissions [6]. It is important here to mention that Kingdom of Saudi Arabia, the world largest fossil fuel based energy supplier was ranked 14$^{th}$ in total carbon dioxide emissions from fossil based fuel combustion, production of cement and gas flaring in 2009[1].

[1] Source: Tom Boden and Bob Andres
Carbon Dioxide Information Analysis Center, Oak Ridge National Laboratory

Gregg Marland
Research Institute for Environment, Energy and Economics, Appalachian State University

| RANK | NATION | $CO_2$_TOT |
|---|---|---|
| 1 | CHINA (MAINLAND) | 2096295 |
| 2 | UNITED STATES OF AMERICA | 1445204 |
| 3 | INDIA | 539794 |
| 4 | RUSSIAN FEDERATION | 429339 |
| 5 | JAPAN | 300282 |
| 6 | GERMANY | 200327 |
| 7 | ISLAMIC REPUBLIC OF IRAN | 164182 |
| 8 | CANADA | 140152 |
| 9 | REPUBLIC OF KOREA | 138908 |
| 10 | SOUTH AFRICA | 136083 |
| 11 | UNITED KINGDOM | 129419 |
| 12 | INDONESIA | 123202 |
| 13 | MEXICO | 121690 |
| 14 | SAUDI ARABIA | 118018 |
| 15 | ITALY (INCLUDING SAN MARINO) | 109309 |
| 16 | AUSTRALIA | 109134 |
| 17 | BRAZIL | 100122 |
| 18 | FRANCE (INCLUDING MONACO) | 99088 |
| 19 | POLAND | 81512 |
| 20 | SPAIN | 78601 |

In 1997, several nations held a climate protection meeting in Kyoto, Japan and drafted the Kyoto Protocol. The ratification of the Kyoto Protocol in 2005 set a goal to reduce the GHG emissions by 5.2 % during 2008 to 2012 compared to the levels of 1990. Unfortunately, the Kyoto conference failed to achieve much regarding the reduction of greenhouse gases emissions and if no measures are taken in the near future the emissions will continue to increase [7].

Currently the available options for reducing carbon dioxide emissions are: (1) reducing the energy consumption via efficient utilization of energy, (2) switching to high hydrogen to carbon ratio fossil based fuels like natural gas, (3) increasing the share of renewable clean energy sources (wind power, solar energy, etc.) in the energy generation and (4) carbon dioxide capture and storage. It is evident that all of the above options must be implemented to reduce carbon dioxide emissions to the desired level. Unfortunately, renewable energy alternatives are not ready yet to replace the fossil based fuels because

of the high cost and the risk involved with those alternatives. Add to that, the disturbance that could result in worldwide economy and energy supply chain form the sudden change to non-fossil based fuels.

Therefore, the world will continue to rely on fossil fuels (oil, coal and gas) in the near future, and according to the international energy agency fossil fuels provide 80% of the world energy demand on the first part of the 21st century [8] (see Figure 5). That's why carbon dioxide capture and storage is considered a promising option for the minimization of carbon dioxide emissions.

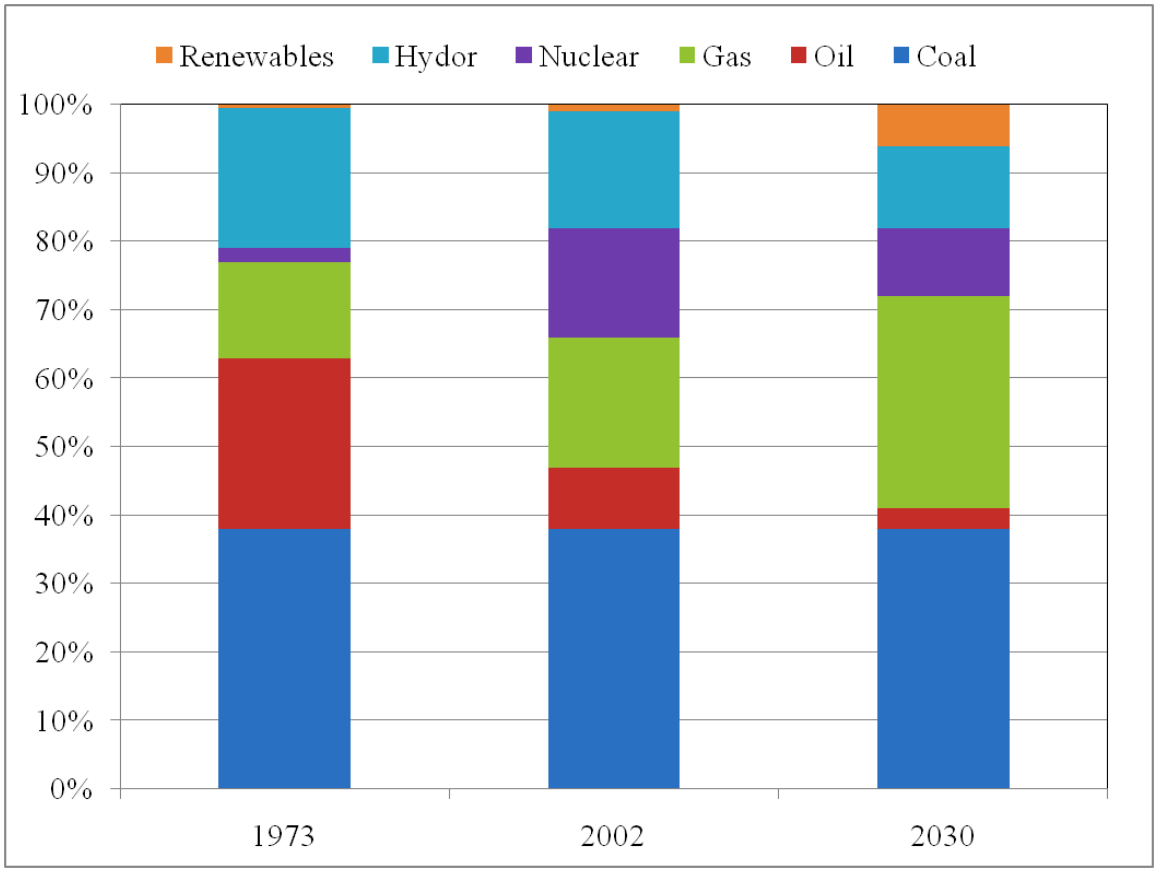


Figure 5: Energy sources by fuel type

Currently, the techniques available for carbon dioxide capture are: (1) pre-combustion capture where the de-carbonization of the fuel is carried out before the combustion process, (2) post-combustion capture, which involves the separation of carbon dioxide from the flue gases resulting from the combustion, (3) oxy-fuel combustion where the fuel is combusted using almost pure oxygen instead of air. However, most of the above mentioned processes are energy intensive, which will result in an increase in the cost of energy and reduce the efficiency of energy generation. On the other hand, the novel chemical looping combustion (CLC) has a high potential as an efficient and economical technology for capturing carbon dioxide without any energy penalty [5], [9]. The main disadvantage of chemical looping combustion is the maturity of the technique since it is an emerging technology, but it must be considered that during the last two decades great efforts have being made by researchers regarding the development of CLC.

The present study deals with the synthesis of Ce modified Ni and Fe based oxygen carriers for the process of chemical looping combustion as developing suitable oxygen carriers is one of the main challenges towards the large scale application of chemical looping combustion.

The oxygen carrier samples were prepared, characterized and finally tested in CREC Riser simulator unit to evaluate the reactivity of the oxygen carriers with different fuel types. Modification of the support with cerium improves both the reactivity and the stability if the oxygen carriers as it will be shown later in the results section.

# CHAPTER 2

# LITERATURE REVIEW

## 2.1 Carbon Dioxide capture techniques

The separation of carbon dioxide from the flue gases is the first step in management and sequestration of carbon dioxide form the atmosphere. As previously mentioned carbon dioxide emissions can be minimized by three capturing technologies: post-combustion techniques, oxy-fuel combustion and pre-combustion/de-carbonization. The selection of the capturing technique will depend on the type of fuel, the gas stream pressure and $CO_2$ concentration in the stream. The bases of the existing technologies are the chemical and physical separation of carbon dioxide which includes adsorption, membrane, absorption and cryogenics.

### 2.1.1 Post combustion

In post combustion capture, carbon dioxide is removed from the flue gases resulting from the fuel combustion process. Since almost 80% of the air is nitrogen and it is used in fossil fuel based power plants for fuel combustion, the concentrations of carbon dioxide in the flow gas will be lower than 15% [4]. Thus, carbon dioxide must be separated from the flue gases as the sequestration of these gases is not practical due the cost and

difficulty of compression and storage. It is difficult to develop and design feasible post capture techniques for removal of carbon dioxide from the flue gases due to the large amounts of gases in which $CO_2$ concentration are very low. Bedside the large size of the equipment thus large capital costs, there is another challenge in the flue gases high temperature. Post combustion capture processes include the use of membranes, chemical absorption and distillation [10].

### 2.1.2 Pre-combustion

Pre-combustion $CO_2$ capture involves de-carbonization of the fuel before the combustion process. A gas mixture of CO and hydrogen fuel can be produced through reaction of fuel with air or steam, which is called gasification process. The syngas mixture is shifted by steam to convert CO to $CO_2$ and generate more hydrogen. Carbon dioxide is separated leaving hydrogen as combustible fuel. For example the typical reactions for coal gasification are [11]:

$$2C + O_2 + H_2O \rightarrow H_2 + CO + CO_2$$

$$C + H_2O \rightarrow H_2 + CO$$

$$CO + H_2O \rightarrow CO_2 + H_2$$

The advantage of pre-combustion capture is the reduction in the cost and size of the separation equipment as a result of the concentrated carbon dioxide stream. However, the high capital cost is the main drawback of this technology.

### 2.1.3 Oxy-fuel combustion

In oxy-fuel combustion the fuel is combusted using almost pure oxygen instead of air, which yields a high concentrated carbon dioxide flue gas stream. Since the flue gas stream is highly concentrated with carbon dioxide only simple carbon dioxide separation is needed if no at all. In addition, the formation of NOx compounds is minimized as a result of the pure oxygen used in the combustion process. The process of providing the pure oxygen for the combustion is the controlling step in determining the cost of the process and the energy penalty.

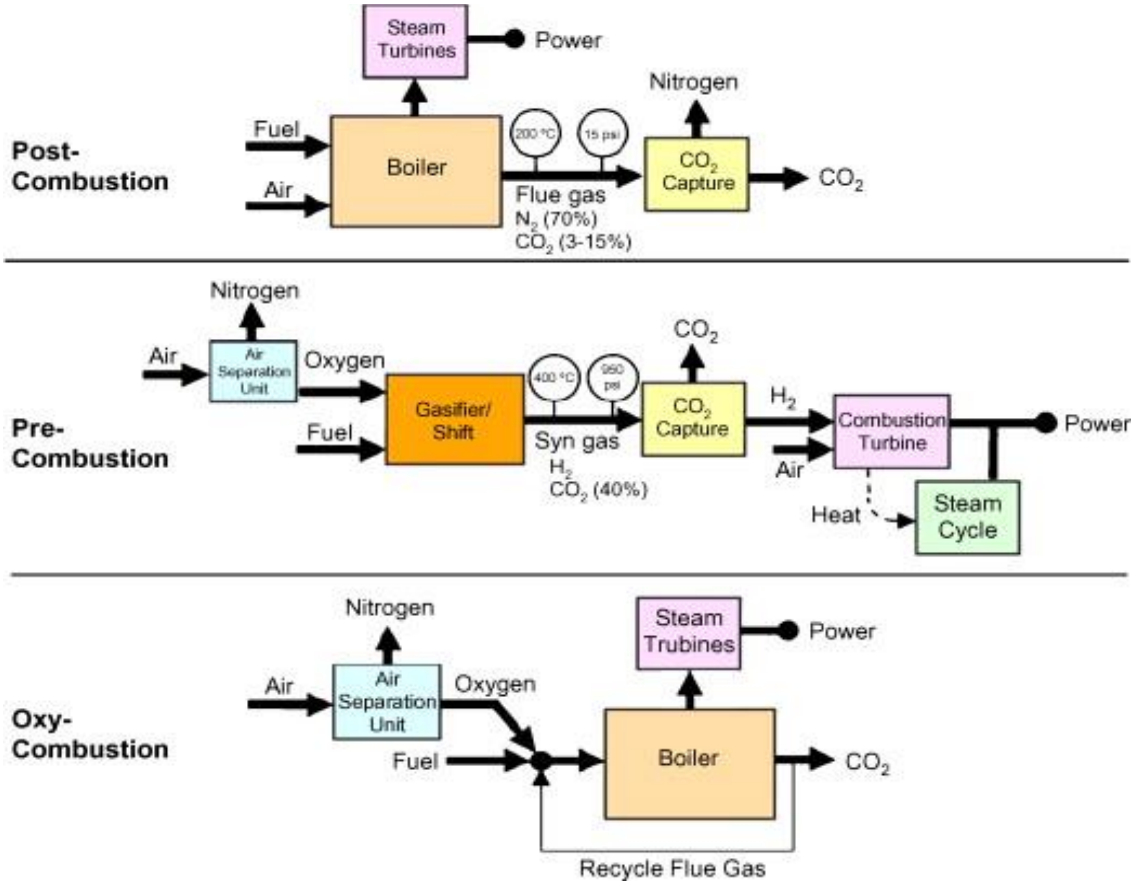


Figure 6: $CO_2$ capture techniques

The bases of the existing separation technologies are the chemical and physical separation of carbon dioxide which includes adsorption, membrane, absorption and cryogenics.

In chemical absorption the chemical solvents will react with carbon dioxide to form intermediate compounds that will be broken when the heat is applied to produce pure carbon dioxide stream. The chemical absorption technology utilizes amine solutions like monoethanolamine (MEA), methyl diethanolamine (MDEA) and diethanolamine (DEA) as absorbents [12]. While, organic solvents such as dimethylether polyethylene glycol, propylene carbonate, sulfolane and methanol are used in physical absorption [13]. The low amount of carbon dioxide that can be absorbed, solvent degradation caused by SOx and NOx compounds, corrosion of the equipment and the high energy needed during the regeneration of solvent are major disadvantages of the previous techniques.

Adsorption techniques rely on the adsorption of carbon dioxide on solid adsorbent including zeolite, activated carbon and alumina molecular sieves, followed by the regeneration of the adsorbent. Also the amount of energy associated with the regeneration is a major drawback of those processes.

Another capture technique is the utilization of porous membranes to separate specific components from a stream. The components can be carbon dioxide from combustion flue gases as in post combustion processes or oxygen from air as in oxy-fuel combustion. The membranes can be made from different materials: organic such as polymers or inorganic as zeolite, metallic, ceramic or carbon [10]. In comparison to the other techniques membranes require less energy and no phase change during the process [4]. On the other

hand, membranes require high selectivity because of $CO_2$ concentration and the low pressure ratio and also they require multi-stage operation and/or recycling of streams.

## 2.2 Chemical looping combustion

The process of Chemical looping combustion (CLC) was first proposed in 1983 by Richter and Knoche [14], where the combustion reaction is carried through two separate intermediate reactions: reduction and oxidation reactions. The two reactions occurred separately inside two fluidized bed reactors connected to each other: the first one is the air reactor and the second is the fuel reactor (Figure 7).

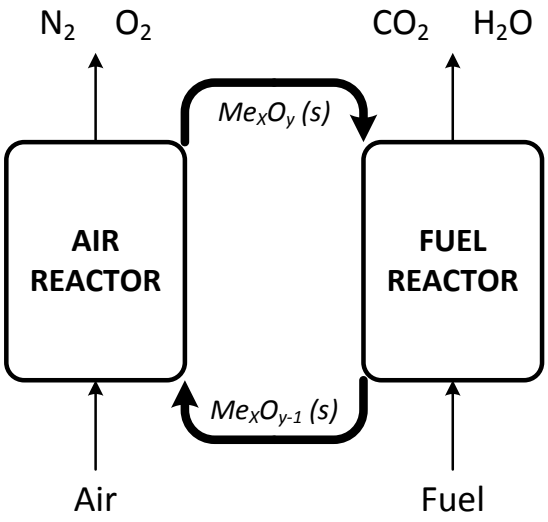


Figure 7: Schematic description of chemical-looping combustion process

Circulating between the fuel and air reactor is the metal oxide (solid) referred to as oxygen carrier which carries the oxygen required for the combustion reaction. In the fuel reactor the feed (fuel) is burned using the oxygen carrier which will get reduced during

the process. The reduced oxygen carrier is re-oxidized by air in the second reactor producing flue gas (only air) that is used to generate energy.

The fuel is fed into the fuel reactor where it will get combusted (oxidized) by the oxygen carrier releasing only carbon dioxide and water vapor (in case of complete combustion) according to the following reaction:

$$C_nH_{2m} + (2n+m)MeO \rightarrow nCO_2 + mH_2O + (2n+m)Me$$

During the combustion reaction the oxygen carrier will be reduced (Me) and then transported to the air reactor, where it will get re-oxidized by air according to the reaction below:

$$O_2 + 2Me \rightarrow 2MeO$$

The gaseous outlet from the air reactor can be sent out to the atmosphere without environmental consequences since the exhaust gas contains only nitrogen and unreacted oxygen.

While in most of the cases the reduction reaction inside the fuel reactor is endothermic, the oxidation of the oxygen carrier is exothermic. The amount of heat absorbed or released during the two reactions depends on the oxygen carrier used as well as the type of fuel. The net amount energy released during both reactions is the same as the energy released during the combustion of fuel with air [9]. Since the oxidation reaction is exothermic, the hot flue gas from the air reactor is used for the production of steam for the generation of energy, and the hot re-oxidized oxygen carrier will supply the required

heat for the combustion reaction. Figure 6 represents a simplified process flow diagram of CLC process [15].

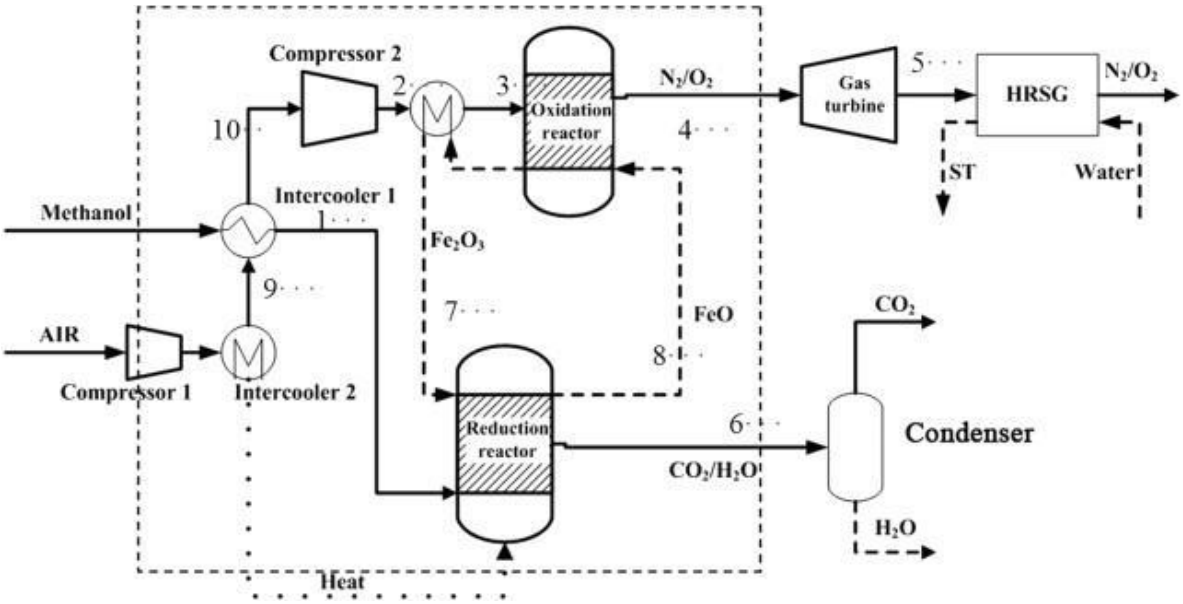


Figure 8: Simplified chemical looping combustion process flow diagram, Source (Moghtaderi, 2011)

Since there are no nitrogen or nitrogen compounds present in the flue gas, the carbon dioxide can be easily captured by condensation of water vapour[9]. Consequently, the application of CLC can successfully eliminate the cost of the additional energy as required by other carbon dioxide separation processes. In addition, the NOx formation in CLC process is also minimal given that the fuel combustion takes place without any flame and the NOx compounds usually form above 1200 ºC, which is CLC maximum temperature [16]. In order to capitalize these advantages, last several years the CLC research received huge attention towards developing matured CLC technologies.

### 2.2.1 Oxygen carriers

The oxygen carrier availability is considered as the main challenge for the chemical-looping combustion to be applied in a large scale. The selection of the oxygen carrier will affect the performance of the CLC system, since the net amount of heat produced relies on the type of metal oxide being used. In addition, the oxygen carrying capacity largely determines the solids (oxygen carrier) circulation rate between the two reactors and the amount of the oxygen carrier in each one of them. The O.C. must possess the following properties [9]:

- High oxygen carrying capacity
- High reactivity in both oxidation and reduction reactions
- Agglomeration resistance
- Adequate fluidization properties
- Attrition resistance
- Stability under reduction/oxidation cycles
- Friendly to the environment
- Low cost.

The development of suitable materials for oxygen carrier has been the center of focus of many researchers in the field of chemical looping combustion. Oxides of transition metals like nickel, copper, manganese and iron have been widely used as active components for oxygen carrier preparation because of their good reduction/oxidation properties [17]–[20]. Also oxides of the above mentioned metals have a high fuel

conversion compared to other metal oxides. These metal oxides can be used directly as oxygen carriers, but often lack the sintering resistance and mechanical strength to withstand the repeated oxidation/reduction cycles [21], [22]. Thus, they are usually supported on materials such as $Al_2O_3$, $NiAl_2O_4$, $MgAl_2O_4$, $SiO_2$, $TiO_2$ and $ZrO_2$.

***Oxygen carrier preparation methods***

Since pure metal oxides often don't have the required properties for making a good oxygen carrier, they are usually supported on inert materials to improve mechanical properties as mentioned before. The supporting material increases the mechanical strength, reduces the attrition rate and provides large surface area for the reaction in case of porous supporting material.

The dispersion of the metal oxide over the supporting material, mechanical stability of the oxygen carrier during the repeated redox cycles and the reactivity of the oxygen carrier, these are the main properties that will be strongly affected by the method used for the preparation. Many preparation methods have been used by the researchers in the synthesis of oxygen carriers. These methods can be ranged from mixing metal oxides and support powders mechanically [23], [24], spray drying [25], freeze granulation [26] and spin flash, and impregnation methods in which active metal solution is impregnated on porous support [27] to precipitation methods such as: sol-gel method [28], solution combustion [29] and co-precipitation.

***Oxygen carriers materials***

*Cu based oxygen carriers*

Copper has some advantages over other material used as oxygen carriers. Copper based oxygen carriers have a high reactivity in reduction and oxidation reactions, no thermodynamic limitations for the complete conversion of fuel to carbon dioxide and water [5], friendly to the environment and also cheaper than the other materials used. However Cu is exposed to agglomeration because of its low melting point [9]. This is clear when pure CuO [30] is used as oxygen carrier; the performance will decreased with the number of oxidation reduction cycles as a result of the agglomeration of the oxygen carrier which will decrease the surface area available for the reduction/oxidation process.

To overcome the stability issues and increase the performance of CuO, several supporting materials have been investigated. Alumina is one of the supporting materials used [31]–[33]. Similar to the case of NiO, interactions between CuO and the alumina support has been reported [33] which will lead to the formation of $CuAl_2O_4$. However, $CuAl_2O_4$ is fully reducible and will not hinder the oxidation reduction performance of the oxygen carrier.

Other supporting materials have been considered such as: $NiAl_2O_4$ [34] which resulted in an increase in the reactivity, but showed lower reduction percentage than NiO. $MgAl_2O_4$ has been also investigated [35] and $ZrO_2$ [24] which showed high reactivity but also high attrition rates and agglomeration at higher temperatures.

*Fe based oxygen carriers*

Iron is one of the most encountered, used and commonly available metals in nature. Also iron is environmentally friendly and nontoxic, add to that its availability and low cost. That's why Fe is commercially attractive for chemical looping combustion application. Performance wise, iron has weak characteristics when it comes to reduction/oxidation cycles, low fuel conversion and low oxygen carrying capacity.

$Fe_2O_3$ has high attrition rate when used unsupported for oxygen carrier application [23]. Alumina has been used as support for $Fe_2O_3$ [26], [35], and the prepared oxygen carriers did not exhibit any agglomeration and the attrition rate was acceptable. High efficiencies for syngas combustion were also reported. Other supporting materials includes: $TiO_2$ [36] and $ZrO_2$ [37]. In most of the applications iron oxide was used pure or mixed with other metal oxides.

*Ni based oxygen carriers*

Despite being toxic and expensive compared to other metals, nickel-based oxygen carriers have been extensively tested in the literature due to their high reactivity and agglomeration resistance as a result of their high melting temperature. Supporting materials have been introduced to improve the mechanical strength, attrition and agglomeration resistances. In this regard, $Al_2O_3$ has been widely investigated as a supporting material for the nickel oxide based oxygen carriers due to the superior fluidization properties and stability [38], [39]. When NiO is deposited on alumina (particularly γ-alumina) always there is a possibility of nickel aluminate ($NiAl_2O_4$)

formation because of the NiO/support interactions [40], [41]. The formation of nickel aluminate ($NiAl_2O_4$) reversely affects the performance of the oxygen carrier because of the lower reactivity and poor fuel conversion.

To avoid the formation of nickel aluminate other supporting materials (α-Al, YSZ and $MgAl_2O_4$) have been introduced considering their low interactions with NiO. That said, these materials must be calcined at high temperatures beyond 1400 ºC to achieve the required mechanical strength. Despite improving mechanical strength, calcination under high temperatures lowers the reactivity by increasing the support/metal interactions and furthermore increases the cost of oxygen carrier preparation[42]. The problem created by the formation of nickel aluminate can be eliminated by using $NiAl_2O_4$ itself as a support for NiO, which is reported to show high reactivity with gaseous fuels, stable performance under high temperature, excellent fluidization properties and agglomeration resistance[43], [44]. While using $NiAl_2O_4$ to support NiO helps improving the performance of the oxygen carrier, it will significantly increase the cost of the oxygen carrier as the support contains nickel compounds, which is expensive compared to other supporting materials.

The task of minimizing the interactions between the support and nickel oxide can also be achieved by chemical treatment of the support. In which the support is coated with other compounds prior to loading the active metal. J.-I. Baek et al. [42] reported that the modification of $\gamma$-$Al_2O_3$ support with MgO improves the oxygen transfer capacity and the performance of the Ni-based oxygen carrier. Also E. Jerndal et al. [25] tested the effects of MgO and CaO addition to α-Alumina support and concluded that the addition MgO to the support prior loading NiO improves the fuel conversion. In another studies Co and La

were found to improve the oxygen carrier reducibility as a result of minimizing the support/metal interactions [40], [45].

### 2.2.2 Chemistry

As mentioned earlier the oxygen carrier generally consists of an active metal oxide loaded on an inert support. The support will provide the high surface area for the metal dispersion and the required mechanical strength to withstand the repeated CLC cycles. The metal oxide which is the active part of the oxygen carrier will participate in the oxidation reduction reactions that represent the combustion process during chemical looping combustion.

Listed below are some of the proposed reaction schemes for some of the common oxygen carriers in chemical looping combustion as reported in the literature [36], [46]–[49].

*Iron*

$$4Fe_2O_3 + CH_4 \rightarrow 8FeO + CO_2 + 2H_2O$$

$$2FeO + \frac{1}{2}O_2 \rightarrow Fe_2O_3$$

$$FeO + H_2 \rightarrow Fe + H_2O$$

$$3Fe_2O_3 + H_2 \rightarrow 2Fe_3O_4 + H_2O$$

$$Fe_3O_4 + H_2 \rightarrow 3FeO + H_2O$$

*Nickel*

$$4NiO + CH_4 \rightarrow 4Ni + CO_2 + 2H_2O$$

$$NiO + H_2 \rightarrow Ni + H_2O$$

$$2Ni + O_2 \rightarrow 2NiO$$

*Copper*

$$CuO + CO \rightarrow Cu + CO_2$$

$$\Delta H = -132.9 \text{ kJ/mol}$$

$$CuO + H_2 \rightarrow Cu + H_2O$$

$$\Delta H = -98.9 \text{ kJ/mol}$$

$$Cu + \frac{1}{2}O_2 \rightarrow CuO$$

$$\Delta H = -149.4 \text{ kJ/mol}$$

$$CuO + CH_4 \rightarrow Cu + 2H_2 + CO$$

*Calcium*

$$CaSO_4 + 4H_2 \rightarrow CaS + 4H_2O$$

$$CaS + 2O_2 \rightarrow CaSO_4$$

$$CaSO_4 + 4CO \rightarrow CaS + 4CO_2$$

$$\Delta H = 174.16 \text{ kJ/mol}$$

*Manganese*

$$6MnO + O_2 \rightarrow 2Mn_3O_4$$

$$\Delta H = -452.3 \frac{kJ}{mol} O_2$$

$$2Mn_3O_4 + \frac{1}{2}CH_4 \rightarrow 6MnO + \frac{1}{2}CO_2 + H_2O$$

$$\Delta H = 51.2 \frac{kJ}{mole} O_2$$

Complex products can be produced as a result of the interactions between the active metal and the support depending on the preparation technique. Formed compounds can be difficult to reduce, which will lead to the deterioration of the oxygen carrier activity under repeated CLC cycles. One of these compounds is the nickel aluminate $NiAl_2O_4$ which will be formed as a result of the interaction between NiO and Alumina support.

### 2.2.3 Reaction kinetics

The performance of chemical looping combustion system is highly influenced by the reaction kinetics of the oxygen carrier/gas systems. Also the reaction kinetics is an important step in the selection and design of the fuel and air reactors for chemical looping combustion.

Huge efforts have been done and several experiments have been performed to determine the kinetics and reactivity of the oxidation and reduction reactions of oxygen carriers.

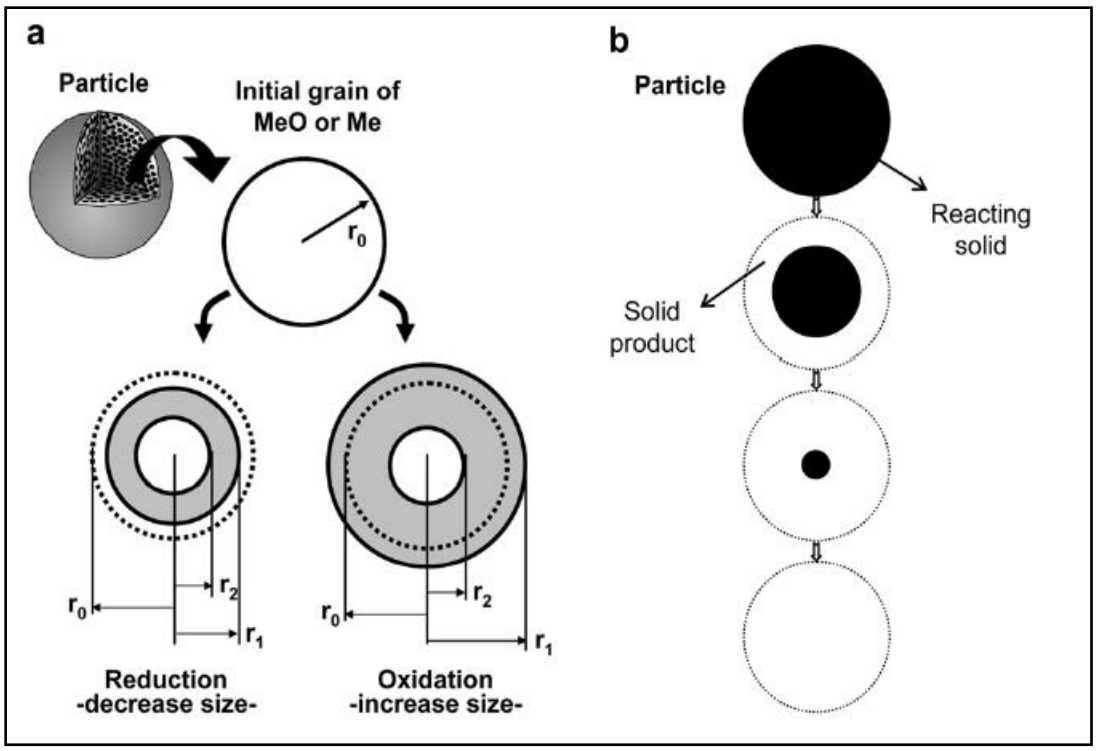


Figure 9: Reaction models in the particle: a) Changing grain size model (CGSM); b) Shrinking core model (SCM), Source (Hossain and de Lasa, 2008)

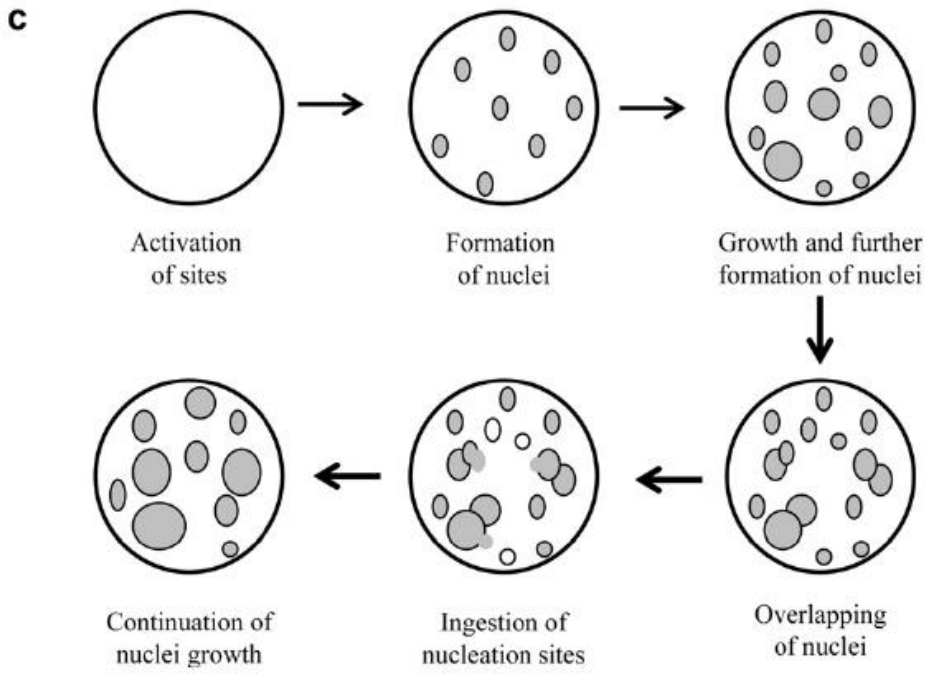


Figure 10: Nucleation growth model, Source (Hossain and de Lasa, 2008)

The reactions occur in the air and fuel reactors can be considered non-catalytic gas/solid reactions [5]. Reviewing the literature one can find several kinetic models, but there are three models that are used frequently: shrinking core models [50], nucleation growth models [51] and the Changing Grain Size Model (CGSM). Figures 9 and 10 show the different reaction steps proposed by the above-mentioned models.

***Changing grain size model (CGSM)***

There are common steps in gas/solid reactions involving: bulk diffusion of the reactants, reactants diffusion inside the pores, adsorption of reactants on the surface of the solid and the chemical reaction [52]. CGSM takes account of the most steps in gas/solid reactions [53]. The model main assumptions are:

- The particle is consisting of non-porous uniform length grains.
- The grain size will change, while the unreacted core will shrink as the reaction takes place.

***Shrinking core model***

The dependency of the solid pore structure and particle size on the rate of reaction is included in the shrinking core model [9]. According to the model the metal/metal oxide interface will move towards the grain center, leaving a porous layer in which the products and reactants will diffuse as the reaction proceeds.

***Nucleation growth model***

According to this model as the reaction proceeds, the metallic nuclei will form and then grow to finally overlap. The increase in the nuclei numbers increases the rate of reaction during the reaction first moments [5]. The reaction will proceed uniformly past this point with the reaction front advancing into the grain inner parts.

# CHAPTER 3

# Objectives

The main objective of the present research is to develop two different oxygen carriers which are NiO/Ce-$\gamma Al_2O_3$ and $Fe_2O_3$/Ce-$\gamma Al_2O_3$. The oxygen carriers should be highly reactive with both the fuel and air and show stable oxygen carrying capacity in repeated CLC cycles. It is also the objective of this research to investigate the reduction kinetics oxygen carriers. The main derive behind this work is the modification of the $\gamma Al_2O_3$ support with Ce to minimize the metal support interactions in addition to the improvement of the dispersion of the metal oxide over the support, which will lead to better reduction oxidation performance.

The specific tasks are to:

- Synthesize Ce promoted Ni and Fe based oxygen carriers.
- Investigate the effects of preparation method and metal loading percentage on the performance of the oxygen carrier.
- Test the stability of the oxygen carriers under repeated oxidation reduction cycles.
- Characterize the oxygen carrier samples through XRD, SEM, BET, TPR, TPO and Pulse chemisorption.
- Evaluate the reactivity of the oxygen carriers with the fuel and air.
- Investigate the reduction kinetics of the oxygen carriers and compare the model to the experimental data.

# CHAPTER 4

# Experimental and methodology

## 4.1 Oxygen carrier preparation

The oxygen carrier samples were synthesized by incipient wetness technique (see Figure 11) using $\gamma$-$Al_2O_3$ as a support, while nickel nitrate, iron nitrate and cerium nitrate were used as sources for nickel, iron and cerium oxides, respectively. For the improvement of the thermal stability, $\gamma$-$Al_2O_3$ was first modified with Ce (1-5 wt. %) before introducing nickel or iron. Although some factors such as: the nature of the support and the preparation method have some effects on the agglomeration and the formation of the metal (nickel/iron) oxide layer, the metal content has the most influence. Consequently, the metal (nickel/iron) loading was varied between 5 to 20 wt. % to avoid sintering and agglomeration [27], [38].

The main steps involved in metal (Ce/Ni/Fe) loading are: impregnation of the support, drying, reduction and calcination. The same procedure is used for Ce, Ni or Fe loading on Alumina. $Ce(NO_3)_2.6H_2O$, $Ni(NO_3)_3.6H_2O$ or $Fe(NO_3)_2.6H_2O$ powder was dissolved in ethanol and the amount of solvent used is 0.8 mL of ethanol for each gram of alumina. The solution was slowly added (by using a syringe) to the alumina support in a sealed conical flask while under vacuum with continuous mixing. The resultant paste was dried

overnight at ambient conditions. After drying, the sample was moved to a fluidized bed reactor located inside a furnace.

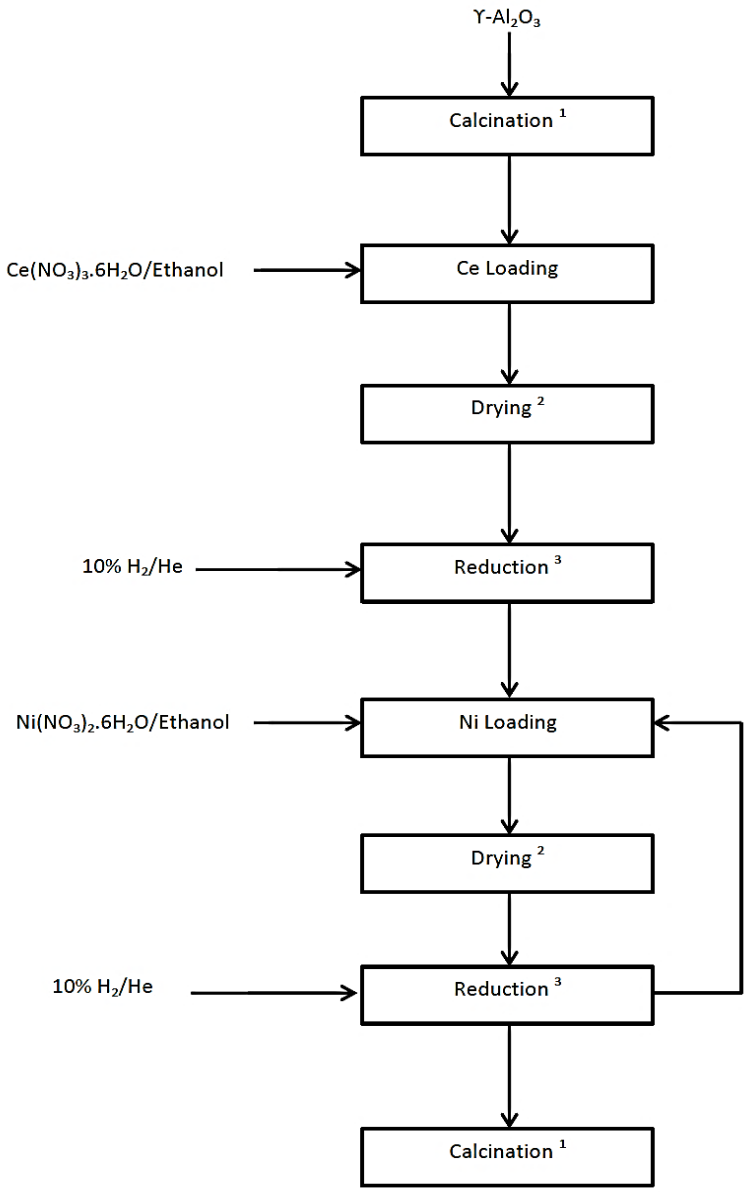


Figure 11: Incipient wetness technique

[2] Calcination at 750 °C
[2] Drying overnight at ambient temperature
[3] Reduction at 750 °C for 8 hrs

The sample was reduced by flowing hydrogen/helium mixture (10% mole fraction hydrogen) under fluidized condition. During the reduction step the temperature was increased from room temperature to 750 $^0$C over 4 hours period and maintained at this temperature for another 8 hours, then brought back to ambient conditions. The thermal treatment process in the presence of hydrogen decomposes the nitrates $Ni(NO_3)_2$ to oxides (NiO and/or $NiAl_2O_4$), and furthermore reducing them to their metallic forms [27]. Illustration of the thermal treatment is presented in Figure 12.

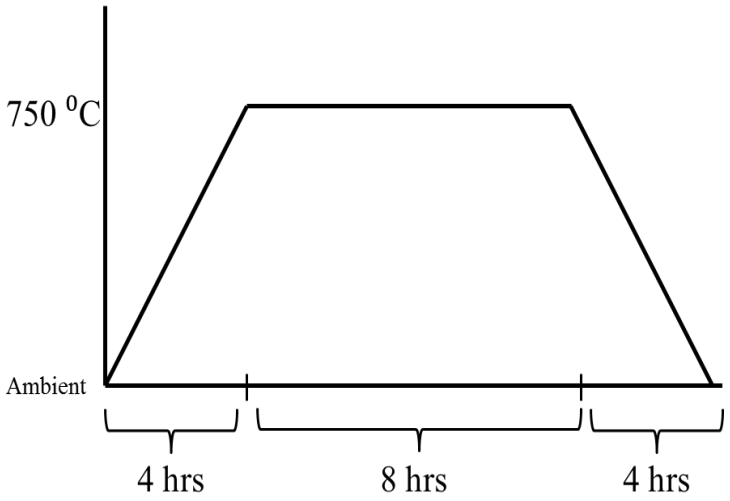


Figure 12: Thermal treatment process illustration

The three steps (support impregnation, drying and reduction) were repeated until 20% metal loading was achieved. In each cycle 5 wt% nickel was loaded to the Ce modified γ-$Al_2O_3$ support. After reaching the 20% nickel loading, the prepared samples were

calcined inside an oven under the flow of air. The temperature was increased to 750 $^0$C applying the same temperature ramp used in the reduction step.

## 4.2 Temperature programmed studies

In this investigation the oxygen carrying capacity and reducibility of the synthesized oxygen carriers were tested using temperature programmed reduction (TPR) and temperature programmed oxidation (TPO) methods. The TPR, hydrogen pulse chemisorption and TPO analysis were performed using "Micromeritics AutoChem II" equipment (Figure 13). For each analysis 0.2 gm of O.C. samples were loaded in a U-tube reactor, which was held inside a furnace.

### 4.2.1 TPR/TPO experiments

Before temperature programmed studies, the sample was pretreated by flowing inert gas (He or Ar). The TPR test was performed using a gas mixture that contains 10% hydrogen in argon circulating through the bed of the prepared sample. The sample was heated to 750 $^0$C from ambient with a rate of 10 $^0$C per minute. Thermal conductivity detector (TCD) was used to analyze the outlet gas concentration. The data from TCD was processed to obtain the hydrogen consumption during the reduction reaction, which was further used to find the metal percentage reduction.

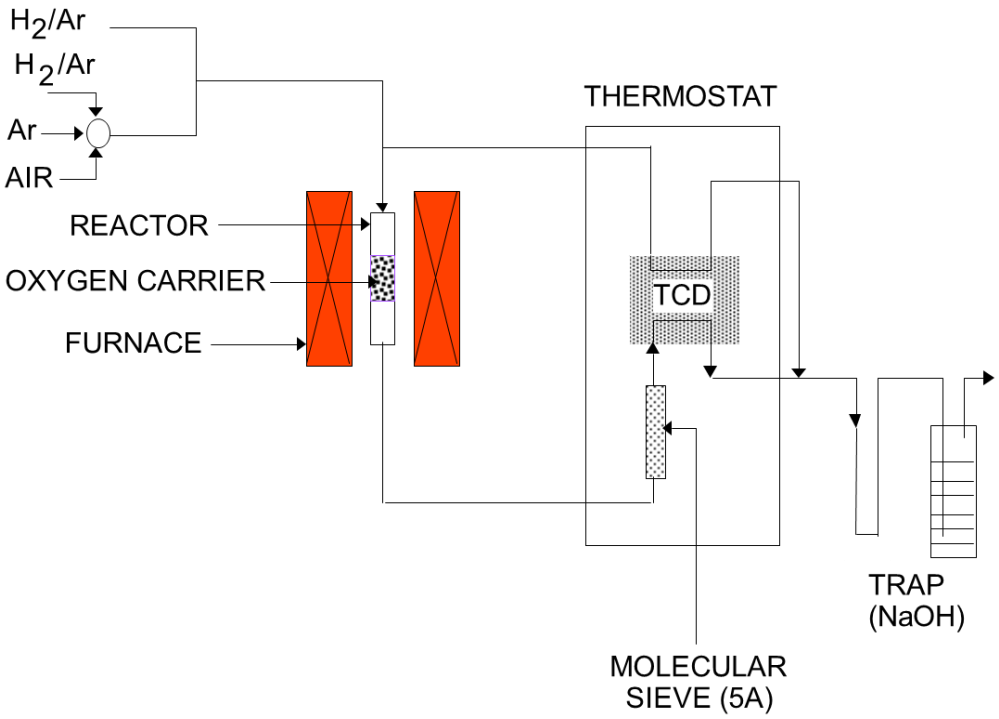


Figure 13: Schematic diagram of AutoChem II

The TPO was conducted to measure metal oxidation percentage. In this test a gas mixture of 5% oxygen in helium was used and the sample temperature was increased to 750 $^{0}$C from ambient with a rate of 10 $^{0}$C per minute. Similar to the TPR, the outlet gas was analyzed using (TCD).

### 4.2.2 Pulse chemisorption

Hydrogen pulse chemisorption tests were carried-out to estimate the percent metal dispersion, average active area and the average particle size. The test was conducted under flowing stream of argon. A series of 1 mL hydrogen pulses were fed to the bed at

ambient temperature. The hydrogen adsorption was analyzed using a TCD detector. The amount of chemically adsorbed hydrogen on the oxygen carrier active sites was used to find the percent metal dispersion, average active area and the average particle size.

## 4.3 CREC Riser simulator

The reactivity, stability and re-generability of the oxygen carriers were established using a CREC Riser simulator operated under the conditions as expected in a large scale fluidized CLC unit (H. de Lasa 1992) [54].

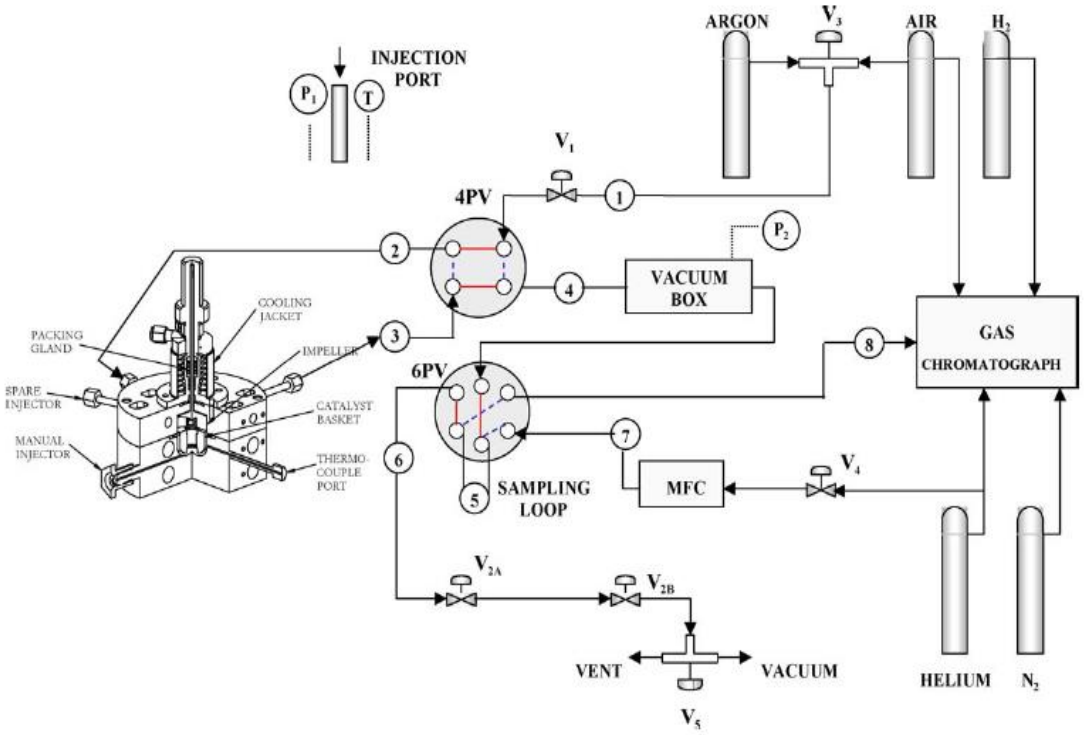


Figure 14: CREC simulator Schematic Diagram, Source (Hossain and de Lasa, 2008)

The CREC Riser simulator (Figure 14) is a bench scale mini-fluidized bed reactor consisting of (i) a 50 ml reactor basket, (ii) heaters (upper and lower), (iii) a vacuum box and (iv) an impeller. The reactor is placed between the upper and lower heaters to maintain uniform temperature of the oxygen carrier bed. The reactor is connected to the vacuum box (1000 ml) by a four port automatic control valve to ensure precise termination of the reaction following pre-specified reaction time. The vacuum box also serves as a product container and directly connected to a GC for product analysis. The impeller, placed on top of the reactor, can rotate upto 7000 rpm speed. The rotation of the impeller forces the gases to flow outward of the impeller center and downward into the reactor annulus, leading to the fluidization of the solid oxygen carrier and ensures intimate contact between gaseous feed and solid oxygen carrier.

For the CLC experiments, 0.5-1 gm of oxygen carrier was loaded in the reactor basket. After leak test, the system was purged with argon to remove the air completely. Meanwhile, the temperature program was started to heat the reactor to the desired temperature (up to 700 °C). During the heating period argon flow was maintained to avoid any interference of air into the system. The argon flow was stopped as the reactor attained to the desired temperature. The reactor was isolated from the vacuum box when it reached to 1 atm pressure. On the other hand, the vacuum box was evacuated to 3.7 psi using a vacuum pump. At this stage the impeller was turned on and feed ($CH_4/C_2H_6$) was injected into the reactor using a preloaded gastight syringe. The pressure profile of the reactor was recorded during the combustion of methane using a pressure transducer. At the end of the pre-specified reaction time the isolation valve was automatically opened up and transferred all the reactor contents into the vacuum box. The abrupt decrease of the

reactor pressure confirmed the complete transfer of the reactor contents and ensured the termination of the reaction after the pre-specified time. Finally, the products were analyzed using gas chromatography. The reduced oxygen carrier was regenerated (oxidized) using a flow of air at a specific temperature during pre-set reaction time.

Finally, the product species was analyzed using a gas chromatograph. Before the next cycle, the oxygen carrier was regenerated using air.

## 4.4 Nitrogen adsorption and XRD

The nitrogen adsorption test was performed to find the specific surface area of the sample, pore volume and average pore radius of the synthesized oxygen carrier samples. The test was carried out at a temperature of 77 K. Prior the analysis the samples were degassed at 200 $^{0}$C for 2 h. The total pore volume was calculated from the amount adsorbed at a relative pressure (P/P0) close to unity.

The oxygen carrier samples phases were obtained by using X-ray diffraction unit (XRD). The oxygen carrier samples were scanned at room temperature and the intensity was analyzed in the range from 10° until 90°. Analysis software was applied to identify the phases.

# CHAPTER 5

# RESULTS AND DISCUSSION

As mentioned in Chapter 4, for this study nickel and iron based oxygen carriers were synthesized using a cerium modified γ-alumina as a support. The prepared oxygen carrier samples are listed below:

Table 1: List of prepared oxygen carrier samples

| No. | Sample ID | Ce loading (wt %) | Ni loading (wt %) | Fe loading (wt %) |
|---|---|---|---|---|
| 1 | NiO(5)/Ce(1)-$\gamma Al_2O_3$ | 1 | 5 | - |
| 2 | NiO(10)/Ce(1)-$\gamma Al_2O_3$ | 1 | 10 | - |
| 3 | NiO(15)/Ce(1)-$\gamma Al_2O_3$ | 1 | 15 | - |
| 4 | NiO/Ce(1)-$\gamma Al_2O_3$ | 1 | 20 | - |
| 5 | NiO(5)/Ce(5)-$\gamma Al_2O_3$ | 5 | 5 | - |
| 6 | NiO(10)/Ce(5)-$\gamma Al_2O_3$ | 5 | 10 | - |
| 7 | NiO(15)/Ce(5)-$\gamma Al_2O_3$ | 5 | 15 | - |
| 8 | NiO/Ce(5)-$\gamma Al_2O_3$ | 5 | 20 | - |
| 9 | $Fe_2O_3$(20)/Ce(1)-$\gamma Al_2O_3$ | 1 | - | 20 |
| 10 | $Fe_2O_3$(15)/Ce(5)-$\gamma Al_2O_3$ | 5 | - | 15 |

Different characterization techniques including: SEM, XRD and BET have been performed in addition to the temperature programmed reduction and oxidation and hydrogen pulse chemisorption to investigate the performance of the oxygen carriers during chemical looping combustion process. The reactivity of the oxygen carrier with gaseous fuel is studied using CREC Riser simulator.

## 5.1 Temperature programmed studies

In this work the TPR experiments were conducted simulating the reduction reactions in the fuel reactor while TPO experiments were performed to simulate the re-oxidation of the oxygen carrier inside the air reactor of a CLC process. Therefore, the successive TPR/TPO cycles basically represent the complete CLC process. The only difference is that TPR/TPO experiments were conducted in a fixed bed while CLC operates in fluidized beds. These techniques are also very effective tools in two different ways: (i) to investigate the changes of the surface and/or bulk reactivity of the samples as a result of variation in composition, promotion, preparation method and preliminary pretreatment, and (ii) qualitative and quantitative analysis of the gas-solid interaction kinetics.

### 5.1.1 Iron based oxygen carriers

The reduction profiles of two oxygen carriers samples, namely: $Fe_2O_3$(20)/Ce(1)-$\gamma Al_2O_3$ and Fe2O3(15)/Ce(5)-$\gamma Al_2O_3$ are presented in the above figure. The samples were

prepared with 20 wt.% and 15 wt.% iron respectively. Looking at the graph it is clear that both oxygen carriers have the same reduction trend. At around 360 ºC there is a slightly narrow peak for the two samples, which corresponds to the reduction of $Fe_2O_3$ to $Fe_3O_4$. The narrow peak is followed by wider peak at about 565 ºC and this peak is attributed to the transition of $Fe_3O_4$ to FeO to Fe [55]. For the second iron sample Fe2O3(15)/Ce(5)-$\gamma Al_2O_3$ the second is slightly wider due to the reduction of some of the cerium oxide species [56].

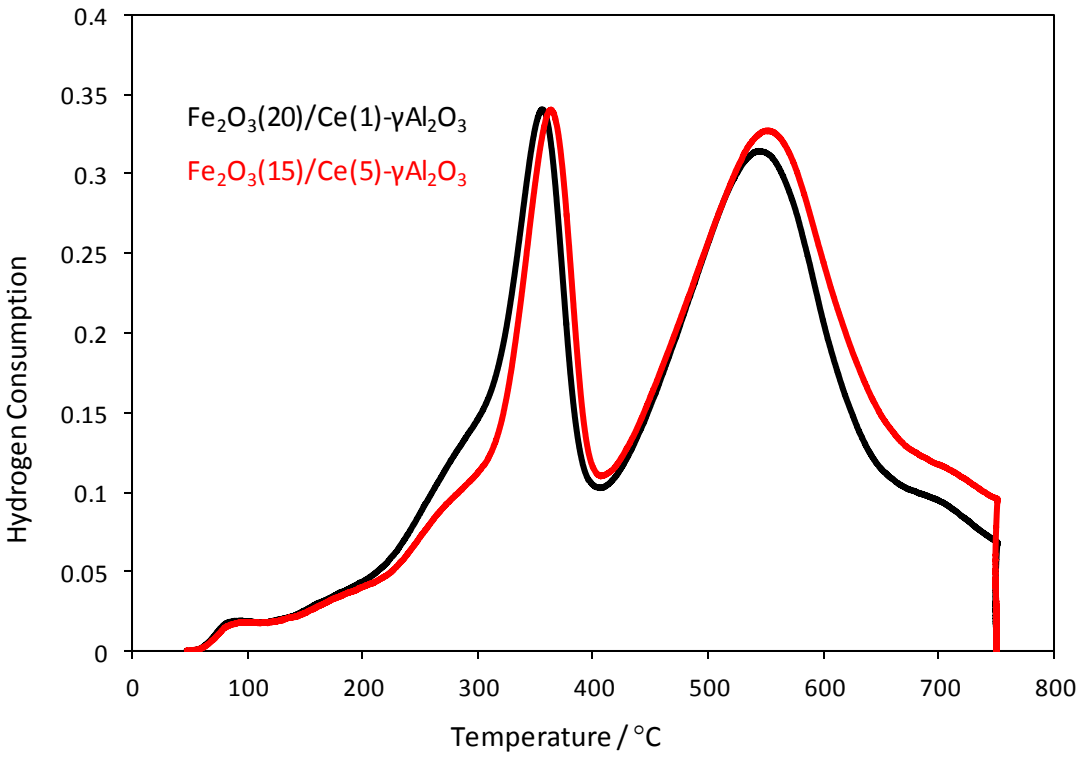


Figure 15: TPR profiles of (i) $Fe_2O_3$(20)/Ce(1)-$\gamma Al_2O_3$ (ii) $Fe_2O_3$(15)/Ce(1)-$\gamma Al_2O_3$ sampels

Successive TPR/TPO experiments were performed to test the oxygen carrier stability for chemical looping combustion. The reduction percentage $Fe_2O_3(20)/Ce(1)-\gamma Al_2O_3$ is around 67% which is understandable for iron based oxygen carriers due to the weak reduction/oxidation properties of the iron oxide [5]. However, for the second sample Fe2O3(15)/Ce(5)-$\gamma Al_2O_3$ the reduction percentage is much higher around 80% as a result of the promotional effects of cerium oxide [57]. Regarding the oxygen carrier stability under repeated reduction/oxidation cycles, both oxygen carriers exhibit stable performance through 9 TPR/TPO cycles as shown in Figure 16 and 17.

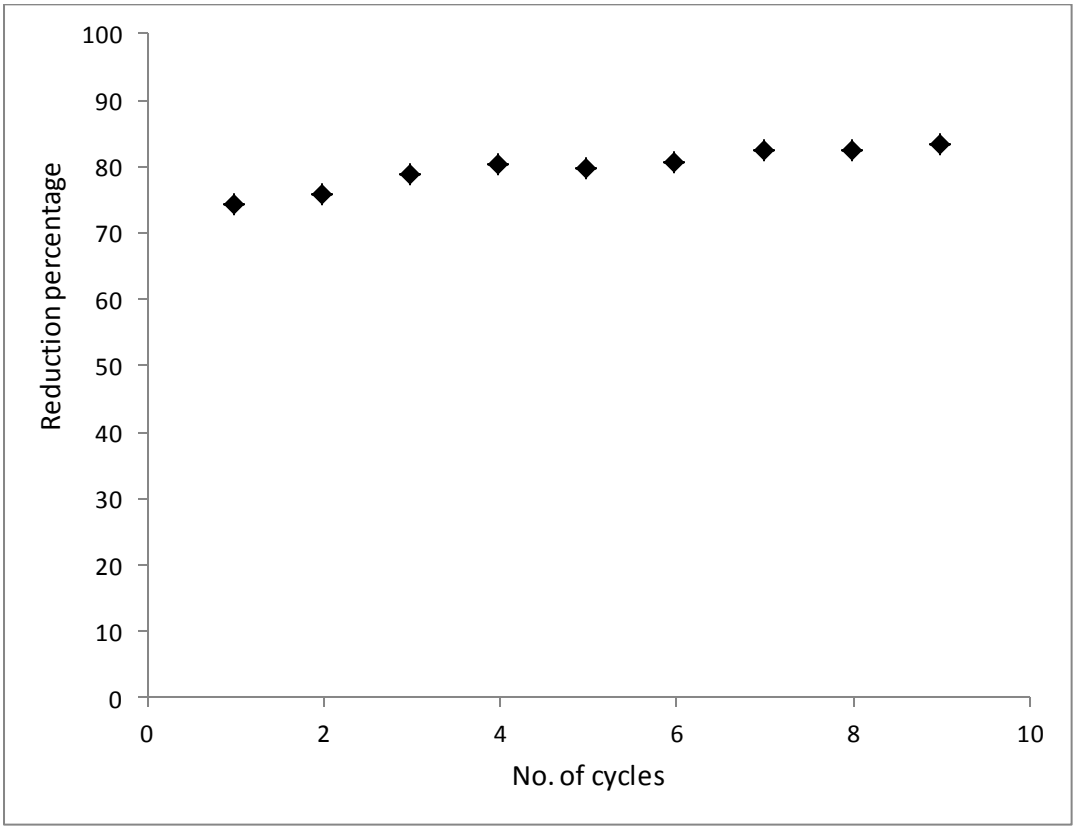


Figure 16: Reduction percentage of $Fe_2O_3(15)/Ce(1)-\gamma Al_2O_3$ under repeated cycles

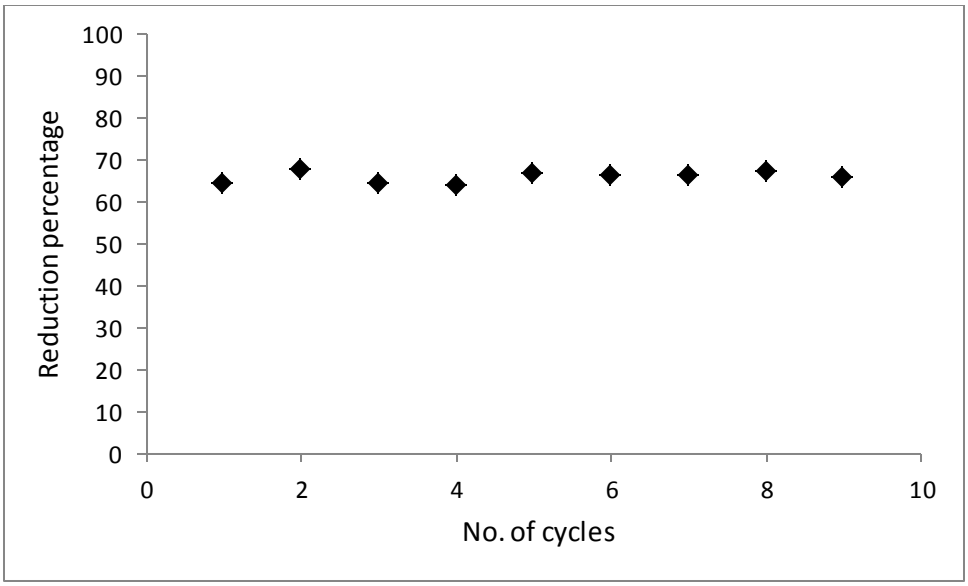


Figure 17: Reduction percentage of $Fe_2O_3$(20)/Ce(1)-$\gamma Al_2O_3$ under repeated cycles

### 5.1.2 Ni based oxygen carriers

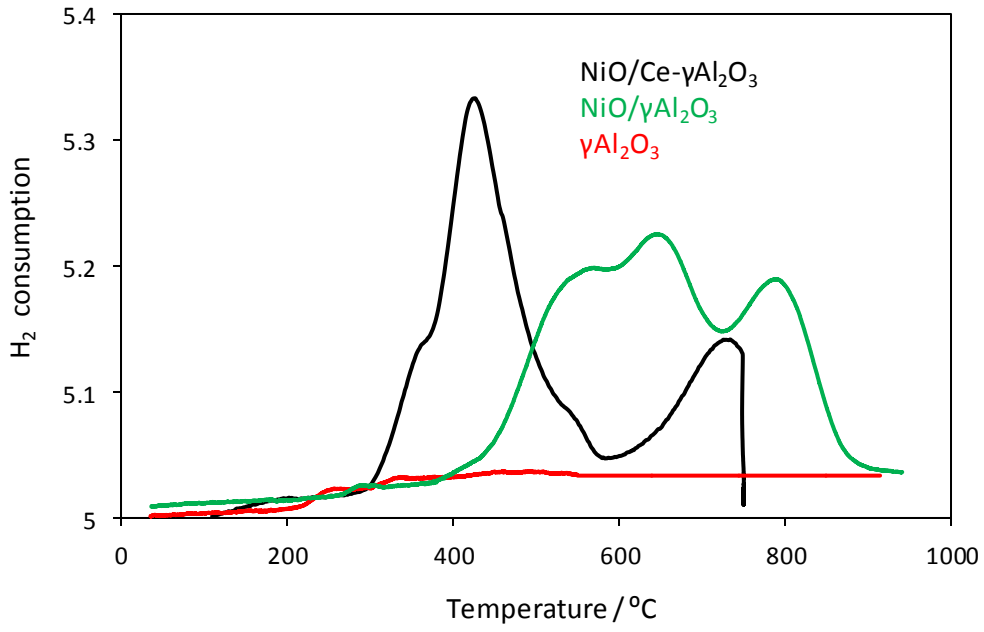


Figure 18: TPR profiles of (i) $\gamma Al_2O_3$ (ii) NiO/$\gamma Al_2O_3$and (iii) NiO/Ce-$\gamma Al_2O_3$ samples

Figure 18 shows the TPR profiles of three different samples (i) $\gamma Al_2O_3$ (only unmodified support), (ii) $NiO/\gamma Al_2O_3$ (nickel on unmodified support) and (iii) $NiO/Ce(1)\text{-}\gamma Al_2O_3$ (nickel on 1 wt % Ce modified support). It is import to mention here that both the unmodified $NiO/\gamma Al_2O_3$ and the Ce modified $NiO/Ce(1)\text{-}\gamma Al_2O_3$ samples were prepared with equal 20 wt% of nickel loading. One can see in the TPR profiles, that the hydrogen consumption by the alumina support (only) is almost negligible which indicates that the support itself does not carry any oxygen during a CLC process. After nickel loading the hydrogen consumption peaks are significantly increased as seen in both the Ce modified and unmodified samples. When the TPR profiles of Ce modified ($NiO/Ce(1)\text{-}\gamma Al_2O_3$) and the unmodified ($NiO/\gamma Al_2O_3$) samples are compared, there are clear distinctions in two aspects, the first is the profiles and the second the area under each curve. In case of the unpromoted sample the peak is broad and appeared at higher temperature. On the other hand for the Ce modified sample the peaks were rather sharp and appeared at lower temperature. For the Ce modified sample the reduction peaks at 421 ºC and 720 ºC represent the reduction of NiO and nickel aluminate ($NiAl_2O_4$), respectively [9], [27], [40]. With the unpromoted sample the reduction peaks of NiO and nickel aluminate are merged into one broad peak. These observations indicate that the addition of Ce helps minimizing the interactions between the active metal oxide and the support leading to the formation of easily reducible nickel oxides. As a result the reduction peak temperature of the Ce modified sample is significantly shifted to lower temperature as compare to the unmodified sample. Similar results were reported by Zhuang et al. 1991 who found that the reduction reaction starts at much lower temperature for cerium doped samples and the activity was also higher [58]. The amount of hydrogen consumption (obtained by the

integration of the area under the TPR profile) by the Ce modified sample is much higher than that of the unmodified sample which further proves the promotional effects of Ce on the oxygen carrier sample.

In order to determine the upper limit of promotional effects of Ce, a second batch of oxygen carrier was prepared with 5 wt % Ce loading keeping the nickel loading as before (20 wt%). Figure 19 represents the TPR profiles of 1 wt% and 5 wt% Ce modified samples. It is interesting to observe that increasing the loading of Ce from 1 wt% to 5 wt%, the height of the peak was significantly decreased. This trend was also observed by Bortolozzi et al. 2014 where he found that the presence of small amounts of cerium enhances the ethanol conversion until the cerium to nickel ratio reaches 0.17 and decreases beyond that [59]. In addition to that an extra small peak at around 600 ºC was also appeared. The small peak at 600 ºC represents the release of the surface oxygen of the cerium oxide.

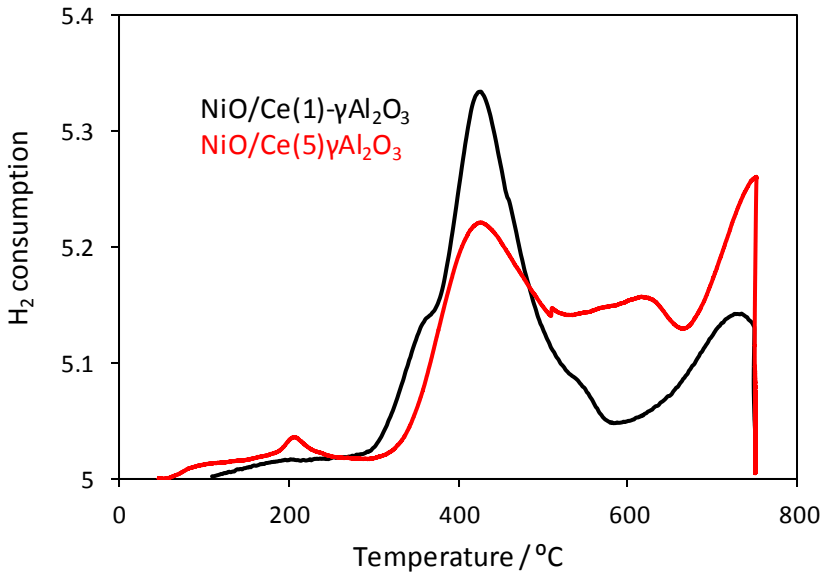


Figure 19: ((TPR profiles of (i)NiO/Ce(1)-$\gamma Al_2O_3$ (ii) NiO/Ce(5)-$\gamma Al_2O_3$ sampels

Those changes suggest the presence of synergetic interactions between the cerium and nickel oxides, which leads to the formation of oxygen species that are only reducible at higher temperatures [55]. This effect is due to the strong metal-support interactions (SMSI) between cerium oxide and nickel in which the cerium oxide covers portions of the metal surface which can affect the reaction and chemisorption properties of the oxygen carrier [60]. SMSI-like interactions between the cerium oxide and nickel were suggested by Chung et al.1984 [61]. In another study Bernal et al. 2003 [62] also indicated that $CeO_2$/metal systems exhibited interactions at temperatures above 773 K that resembles the SMSI previously reported for $TiO_2$/metal systems. Additionally Wrobel et al. 1993 [63] reported that with Ni/Ce ratios larger than 0.5 NiO particles mixed with cerium oxide smaller grains.

The total amount of reducible nickel species was determined from the consumed hydrogen during TPR using the following equation:

$$W_{Ni} = \frac{MW_{Ni} V_{H_2}}{\nu \rho_g} \qquad 1$$

where, $W_{Ni}$ is the weight of reducible nickel species, $MW_{Ni}$ the molecular weight of nickel, $V_{H2}$ the volume of the consumed hydrogen at STP, $\rho_g$ the gas molar volume and $\nu$ is stoichimetric number based on reaction stoichimetry. During TPR of nickel based sample one can consider the following reaction:

$$NiO + H_2 \rightarrow Ni + H_2O$$

Therefore, to reduce one of NiO one mole of hydrogen is required. Finally, the percent of nickel oxide reduction was calculated according to the following equation:

$$\% \text{ Reduction } = \frac{W_{Ni}}{W} \times 100 \qquad (2)$$

where, $W_{Ni}$ is the weight of reducible nickel species, W the actual amount of metal in the catalyst.

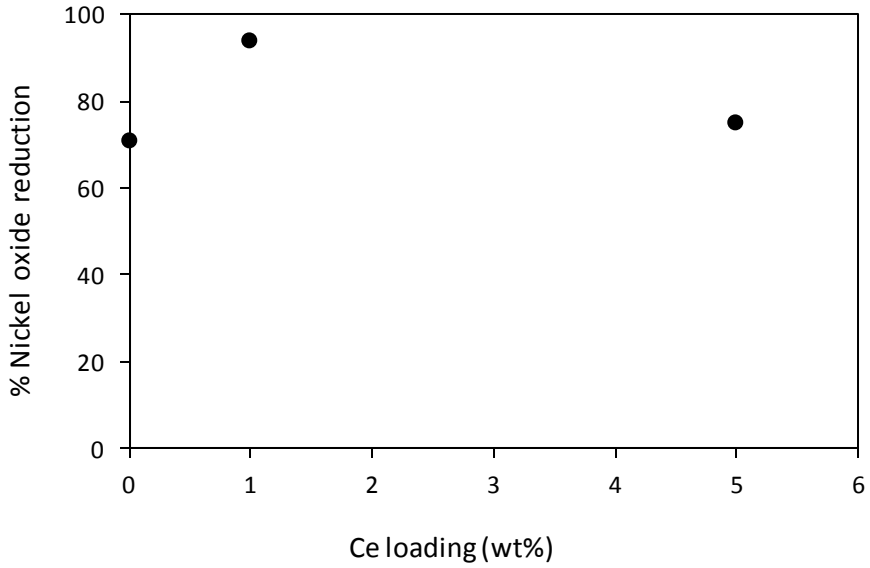


Figure 20: Effect of Ce modification on percent of nickel oxide reduction

Using Equation (2) the percent of nickel oxide reduction was calculated and Figure 20 shows the reduction percentage for NiO/$\gamma Al_2O_3$, NiO/Ce(1)-$\gamma Al_2O_3$ and NiO/Ce(5)-$\gamma Al_2O_3$ to show the effect of increasing the percentage of Ce modifier.

The reduction percentage of NiO/$\gamma Al_2O_3$ is 71% as a result of the formation of poorly reactive nickel aluminate due to the interaction between the support and the nickel oxide. In addition, the calcined unpromoted NiO/$\gamma Al_2O_3$ oxygen carriers were reported to

contain poorly crystalline nickel oxide particles [64]. Modification of the alumina support with 1 wt% Ce increases the amount of easily reducible NiO while reducing the formation of $NiAl_2O_4$ as a result of the minimization of the interaction between the metal oxide and the support, as suggested by Xavier et al. 1999 [57]. As a result, the percentage reduction increases to 94%. The further increase of Ce to 5 wt% brought down the reduction percentage to 75% as a result of the synergistic interactions between Ce and Ni leading to the formation of less reactive oxygen species as mentioned before. Besides that, increasing the cerium percentage means increasing the metal loading which increases the agglomeration of OC samples [38].

Based on the TPR analysis as discussed above, NiO/Ce(1)-$\gamma Al_2O_3$ sample was selected for further evaluation in repeated TPR/TPO cycles. The cyclic TPR/TPO experiments were used to measure the percentage reduction and the oxygen carrier stability over multiple redox cycles. As mentioned above, the TPR/TPO cycles represents the repeated combustion and regeneration reactions during CLC process.

Figure 21 plots the percentage reduction for NiO/Ce(1)-$\gamma Al_2O_3$ during the repeated TPR/TPO cycles. One can see that the percentage reduction remains almost unchanged around 94% through the reduction/oxidation cycles, which is an indication the oxygen carrier stability under the repeated redox cycles and the absence of agglomeration. The oxygen carrier stable activity further confirms the promotional effects of the cerium which prohibits the formation of nickel aluminate and the transformation of $\gamma$- $Al_2O_3$ to $\alpha$- $Al_2O_3$ which causes the support to lose the high surface area and mechanical strength and leads to deactivation [42], [65]. Not to mention that, the presence of cerium decreases the carbon deposition over the oxygen carrier [58], [66].

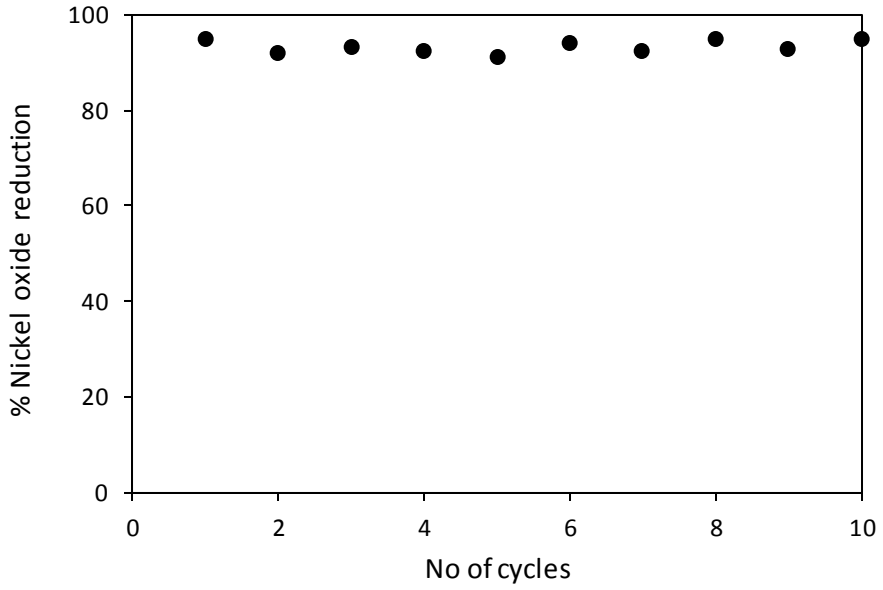


Figure 21: Percent of nickel oxide reduction of NiO/Ce(1)-$\gamma Al_2O_3$ sample over repeated TPR/TPO cycles

## 5.2 Oxygen carrier characterization

The nickel based oxygen carrier samples were chosen for further investigation based on the previous results. The oxygen carrier characteristics: pore size and volume and the specific surface area are very important properties when it comes to determining the active sites distribution, reactivity and adsorption capacity of the oxygen carrier and the probability of sintering deactivation of the carrier. The active sites dispersion, reactivity and adsorption capacity of the oxygen carrier will improve largely with the increase in the specific surface area of the oxygen carrier [56]. $N_2$ adsorption was used to calculate the specific surface area, pore diameter and pore volume of the prepared oxygen carrier samples.

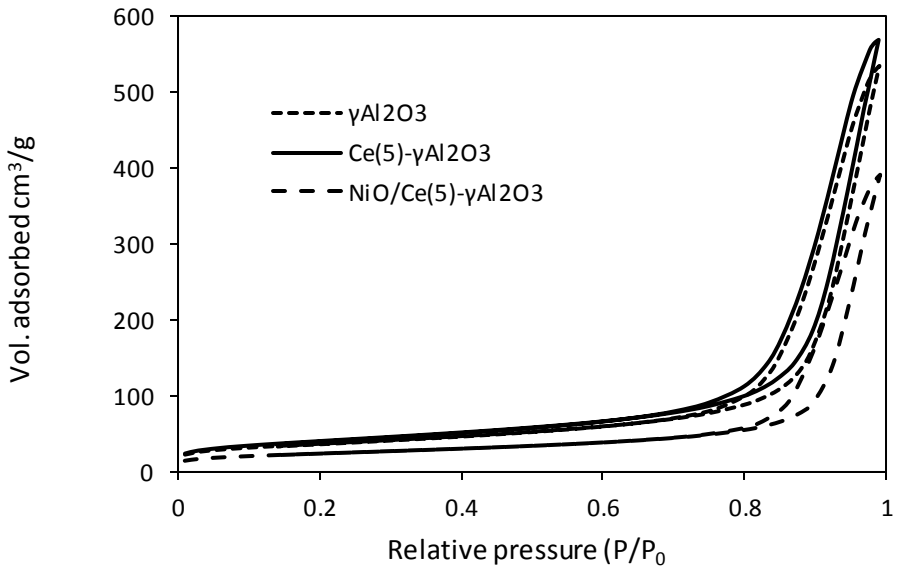


Figure 22: $N_2$ adsorption isotherms

Table 2: $N_2$ adsorption results

| Sample | BET Area ($m^2/g$) | Average pore size (nm) | Vm $cm^3/g$ STP | Vp $cm^3/g$ STP |
|---|---|---|---|---|
| Calcined $\gamma Al_2O_3$ | 148.75 | 19.82 | 34.17 | 0.74 |
| Ce(1)-$\gamma Al_2O_3$ | 134.53 | 21.89 | 30.90 | 0.74 |
| Ce(5)-$\gamma Al_2O_3$ | 135.15 | 21.16 | 31.05 | 0.72 |
| NiO/Ce(5)-$\gamma Al_2O_3$ | 89.42 | 21.73 | 20.54 | 0.49 |

The values of specific surface area, average pore size and pore volume values are listed in Table 2. The surface area was calculated using BET equation form the linearity of the

adsorption isotherms between relative pressure values of 0.05 to 0.4 as shown in Figure 22. Looking at the nitrogen adsorption isotherms one can see that the adsorption isotherms are of IV profile type, which is common among mesoporous solids. Also it is clear that the pore structure was altered after nickel loading.

After modification of the support with Ce the specific surface area decreased to about 135 $m^2/g$, and further decreased after nickel loading. But still with a value of 89.42 $m^2/g$ the surface area is much higher than the surface area of $\alpha Al_2O_3$ and this indicates there is no phase transformation of the $\gamma Al_2O_3$ support, which is crucial to the oxygen carrier stability and deactivation resistance, because $\alpha Al_2O_3$ has less surface area and mechanical resistance compared to $\gamma Al_2O_3$. While the loading of the cerium and nickel had no significant effect on the average pore size, the reduction on pore volume was noticeable after nickel loading.

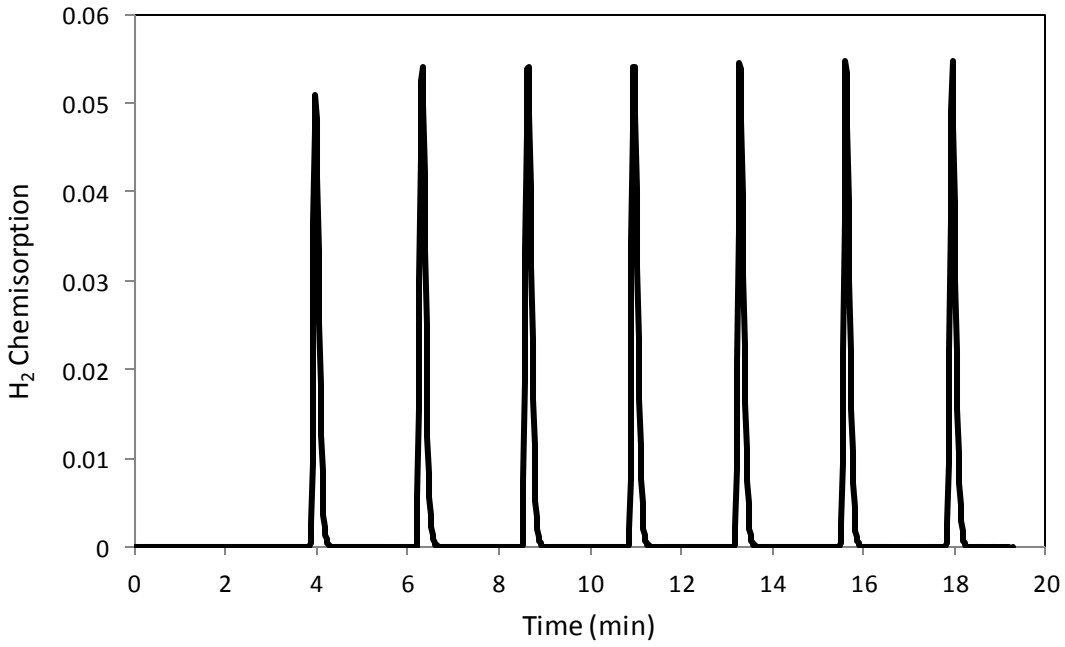


Figure 23: Pulse chemisorption profile

Table 3 summarizes the results of hydrogen pulse chemisorption analysis as obtained for oxygen carrier samples after the first reduction cycle and after 10 TPR/TPO cycles. Typical pulse chemisorption profile is shown in Figure 23, where hydrogen pulses were injected to the oxygen carrier sample to be chemisorbed and the excess hydrogen volume was recorded to calculate the dispersion and crystal size. The chemically adsorbed hydrogen on the catalyst active sites is used in the calculation of the dispersion percentage according to the following equation:

$$\%D = \frac{CX}{Wf} \qquad 3$$

where C is a constant, X is the total chemisorbed hydrogen, W is the percentage of weight metal and f is the reduced metal fraction. The crystal average size ($d_v$) can be estimated using the following formula:

$$dv = \frac{\varphi V_m}{S_m} \times \frac{1}{\%D} \qquad 4$$

where, $\varphi$ is the particle shape constant, $S_m$ is the average surface area of the exposed metal surface per metal atom surface, $V_m$ is the volume of metal atoms. The addition of cerium oxide improves the surface area and the dispersion of the nickel, which enhances the oxygen carrier reducibility as confirmed by Liu et al. 2008 [67]. But apparently, increasing the percentage of Ce has minimal impact on the metal dispersion as can be seen from Table 3.

Table 3: Dispersion and crystal size results

| Sample | TPR/TPO cycle (No.) | Dispersion (%) | Crystal size (nm) |
|---|---|---|---|
| NiO/Ce(1)-$\gamma Al_2O_3$ | 1 | 1.86 | 50.4 |
| NiO/Ce(1)-$\gamma Al_2O_3$ | 10 | 1.67 | 50.7 |
| NiO/Ce(5)-$\gamma Al_2O_3$ | 1 | 1.63 | 51.5 |
| NiO/Ce(5)-$\gamma Al_2O_3$ | 10 | 1.64 | 51.9 |

However, one can see that both the metal dispersion and nickel crystal sizes remained stable over the repeated TPR/TPO cycles, which further confirms the oxygen carrier stability under the repeated oxidation/reduction cycles and the absence of agglomeration.

The uniform dispersion of the metal oxide over the support was further confirmed using SEM mapping as presented in the following figure:

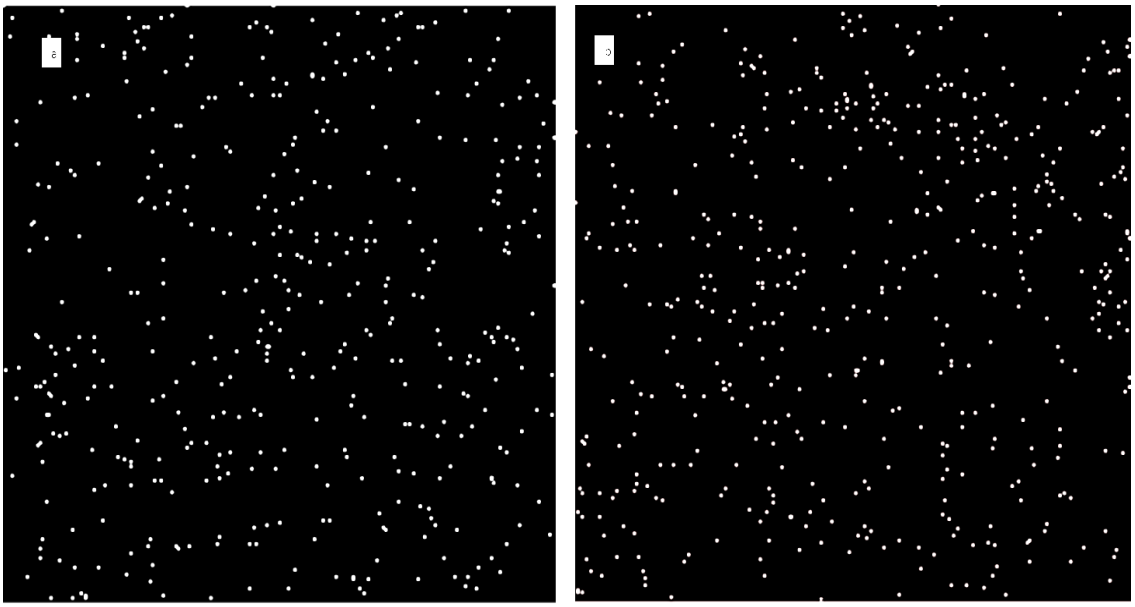

Figure 24: SEM mapping for NiO/Ce(1)-$\gamma Al_2O_3$ (left) nd NiO/Ce(5)-$\gamma Al_2O_3$ (right)

## 5.3 X-ray diffraction test

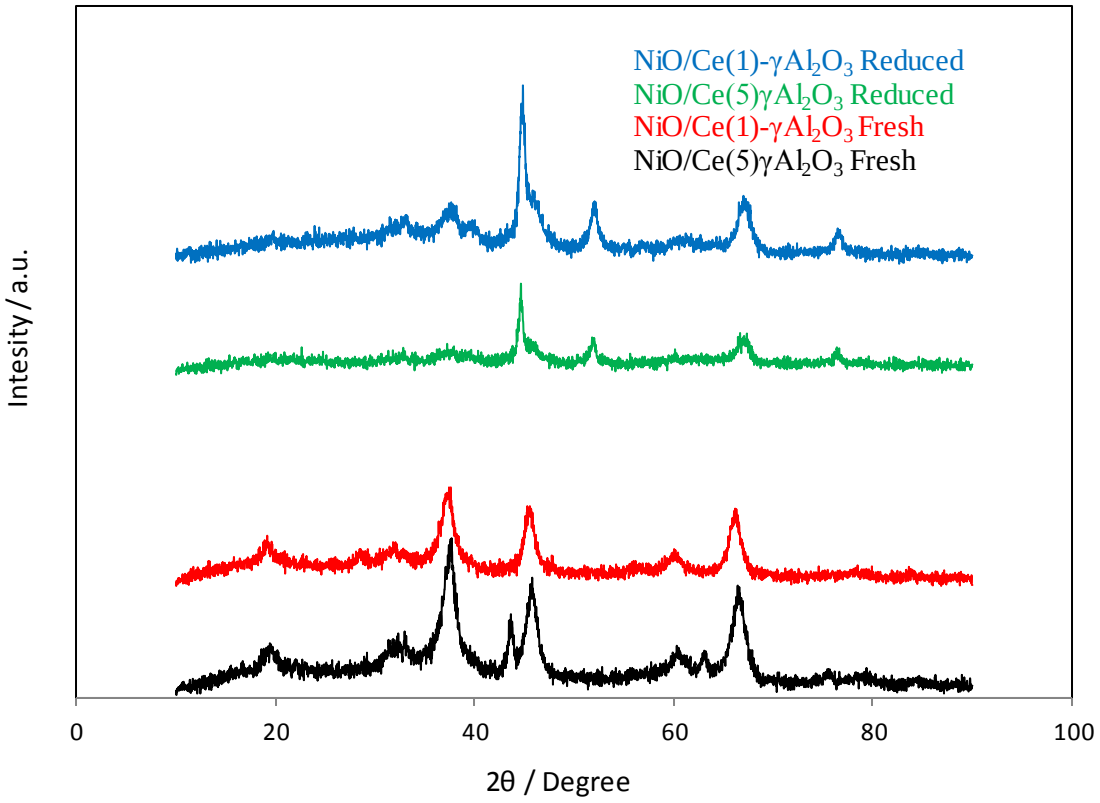


Figure 25: XRD Patterns of the prepared oxygen carriers

Figure 25 presents the X-ray diffractograms of fresh NiO/Ce(1)-$\gamma Al_2O_3$ and NiO/Ce(5)-$\gamma Al_2O_3$ samples and the reduced samples after 10 TPR/TPO cycles. XRD test results didn't show any peaks corresponding to CeO2 or CeAlO3, which indicates a uniform dispersion of the cerium phases on the support, and also this could be as a result of the relatively low concentration of Ce. For all samples the XRD diffraction peaks at 19.4°, 31.9°, 45.6° 60.5°, and 66.4° corresponds to the $\gamma Al_2O_3$ and this confirms that $\gamma Al_2O_3$ support was not transformed to $\alpha Al_2O_3$ and explains the stability of the oxygen carrier over the repeated cycles [65].

For the fresh samples the lines at 37.6°, 43.5° and 75.8° are comparable to nickel oxide crystals. However, in the case of fresh NiO/Ce(5)-$\gamma Al_2O_3$ the diffraction line at 43.5° disappear. This could be a result of the coupling of the two peaks at 43.5° and 45.6° for NiO and $\gamma Al_2O_3$ respectively into one peak and similar results have been observed by others[65], [68]. The peaks at 37.6°, 45.6° and 60.5° cold be traced back to nickel aluminate and to confirm whether there is a presence of $NiAl_2O_4$ on the oxygen carrier or not, the oxygen carrier samples were reduced at 750 °C before performing XRD experiments. Based on the XRD results of the reduced samples both showed peaks at 44.7°, 52.1° and 76.5° which correspond to the reduced nickel (Ni). Since the reduced samples only showed peaks for $\gamma Al_2O_3$ and Ni, this indicates that most of the nickel oxide loaded on the support was reduced and this not possible for $NiAl_2O_4$ which cannot be reduced at this temperature. Those findings confirm the absence of nickel aluminate species on the oxygen carrier.

XRD results indicate the formation of easily reducible NiO species over the γ-alumina support, which didn't transform into the less stable $\alpha Al_2O_3$ during the preparation of the oxygen carrier. Also the absence of NiO or $NiAl_2O_4$ peaks on the reduced samples confirms the superior reduction properties of the oxygen carrier samples.

## 5.4 Solid state reduction kinetics

The oxidation and reduction reactions of the oxygen carrier are considered as a multiple steps process. And similar to heterogeneous reactions, diffusion, adsorption and reaction

steps are included in the overall rate of reaction. Which step or steps are controlling the overall reaction depends on the properties of the reducible compounds.

The intrinsic kinetics of temperature programmed reduction can be formulated under the consideration of the overall rate of reaction to be a function of the gas phase composition and the reduction degree of the solid material f(α) [68], [69].

$$\frac{d\alpha(t)}{dt} = k(T) f(\alpha) f(p_{H_2}, p_{H_2O}) \quad (5)$$

where α represents the reaction progress, which can be calculated as follows:

$$\alpha(t) = \frac{\Delta n_t}{\Delta n_{total}} \quad (6)$$

where in case of TPR, $\Delta n_t$ is the hydrogen consumption at time t, and the total number of moles consumed is $\Delta n_{total}$.

The rate constant k is calculated using:

$$k = k_0 \exp\left[\frac{-E_a}{R}\left(\frac{1}{T} - \frac{1}{T_p}\right)\right] \quad (7)$$

Where $E_a$ is the energy of activation, R the global gas constant and $T_p$ is the peak centering temperature. The function $f(p_{H_2}, p_{H_2O})$ can be taken as a constant given that there is no water in the hydrogen, same hydrogen flow rate for all TPR experiments and differential conversion, which will reduce equation (6) to:

$$\frac{d\alpha(t)}{dt} = k_0 \exp\left[\frac{-E_a}{R}\left(\frac{1}{T} - \frac{1}{T_p}\right)\right] f(\alpha) \quad (8)$$

Using Avarmi-Erofeyev model for random nucleation:

$$f(\alpha)=1-\alpha \qquad 9$$

Substitution of equation 7 will lead to:

$$\frac{d\alpha(t)}{dt}=k_0 \exp\left[\frac{-E_a}{R}\left(\frac{1}{T_0+\beta t}-\frac{1}{T_p}\right)\right](1-\alpha) \qquad 10$$

$T_0$ is the initial temperature and $\beta$ is the temperature ramping rate.

Mathematica 8.0 was used to fit the experimental data and find the activation energy and the reaction rate constant ($k_0$).

Figure 26 and 27 display a comparison between the experimental conversion of the nickel particles and the random nucleation model (RNM) for NiO/Ce(1)-$\gamma Al_2O_3$ and NiO/Ce(5)-$\gamma Al_2O_3$ samples respectively. It is clear from the figure that the random nucleation model adequately fits the experimental data.

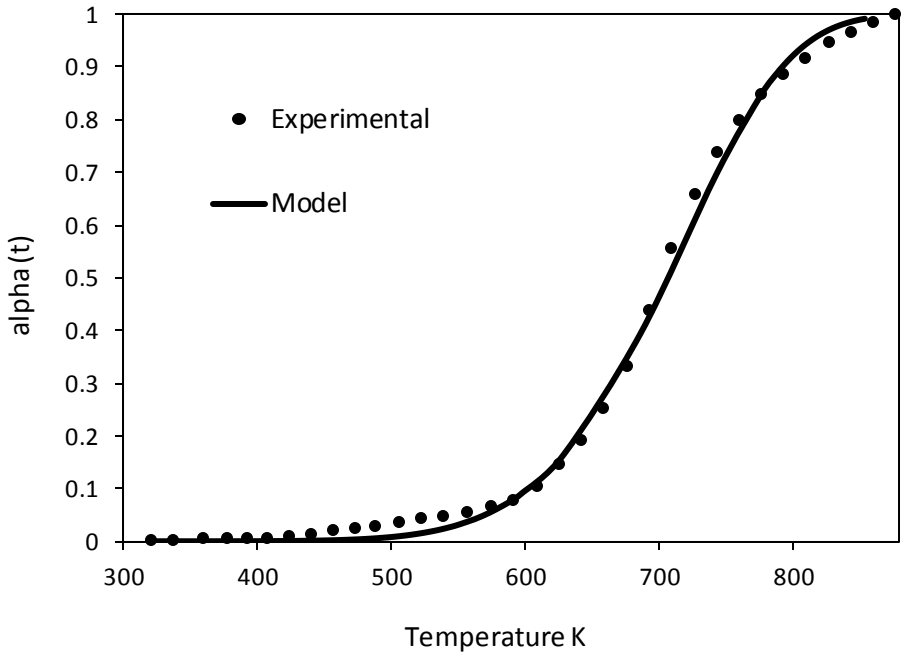


Figure 26: Experimental versus model predicted conversion of nickel oxide (alpha) using NiO/Ce(1)-$\gamma Al_2O_3$ oxygen carrier

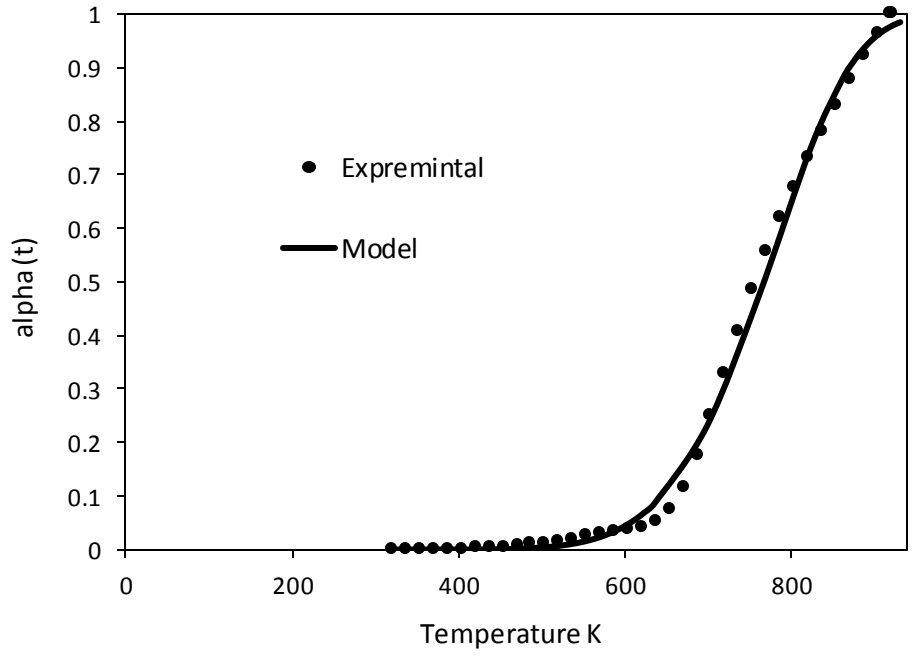


Figure 27: Experimental versus model predicted conversion of nickel oxide (alpha) using NiO/Ce(5)-$\gamma Al_2O_3$ oxygen carrier

The activation energy ($E_a$) was found to be 52.4 ± 0.3 kJ/mol and 52.3 ± 0.2 respectively, which are close to the values reported in the literature as compared in Table 4.

Table 4: Activation energy for the reduction of nickel oxide

| Sample | Reactant | Ea (kJ/mol) |
|---|---|---|
| NiO/Ce(1)-$\gamma Al_2O_3$ | $H_2$ | 52.4±0.3 |
| NiO/Ce(1)-$\gamma Al_2O_3$ | $H_2$ | 52.3±0.2 |
| NiO/$\gamma Al_2O_3$[a] | $H_2$ | 53.5±2.0 |
| NiO/Co(0.5)-$\gamma Al_2O_3$[a] | $H_2$ | 45.1±2.0 |
| NiO(60)/Bentonite[b] | $CH_4$ | 57.0 |
| NiO(65)/$\gamma Al_2O_3$[c] | $CH_4$ | 55.0 |
| [a] ((Hossain et al. 2007[68])) [b] ((Son et al. 2006[70])) [c] ((Moghtaderi et al. 2010[71])) | | |

## 5.5 CREC Riser simulator reactivity studies

The reactivity of the oxygen carrier samples with gaseous fuel (methane/ethane) was tested using CREC Riser simulator unit. The combustion reactions were performed at various temperatures and after each combustion reaction the oxygen carrier was re-generated by following air for 10 minutes at a temperature of 550 ºC. Several combustion and re-generation cycles were performed using the same oxygen carrier sample to test the stability of the oxygen carrier over multiple chemical looping combustion cycles.

The reaction temperature was varied between 550 ºC to 650 ºC, while the contact time was in the range between 10 to 60 seconds.

### 5.5.1 Iron based oxygen carriers

Iron based oxygen carrier sample $Fe_2O_3(20)/Ce(1)-\gamma Al_2O_3$ was reacted with ethane at 550 C° and the contact time was 60 seconds. The pressure profile inside the reactor during the combustion process is presented in the figure below.

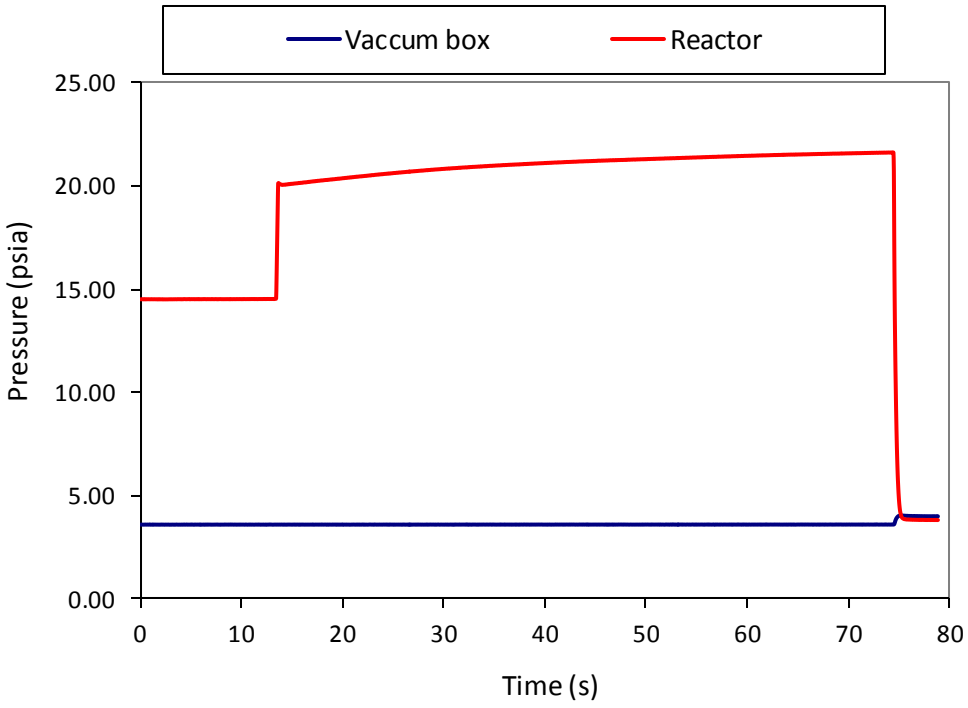


Figure 28: Pressure profile during the combustion process for $Fe_2O_3(20)/Ce(1)-\gamma Al_2O_3$

The pressure inside the reactor was kept at 14.7 psi at the start and the vacuum box was at 3.7 psi. The pressure is increased immediately as the fuel (ethane) is injected into the reactor. After the injection there is a slight gradual increase in the pressure as a result of the formation of the products. The valve between the reactor and the vacuum box was opened immediately at the end of reaction time to insure the reaction was terminated.

Opening the valve between the reactor and the vacuum box the pressure is dropped to about 4 psi.

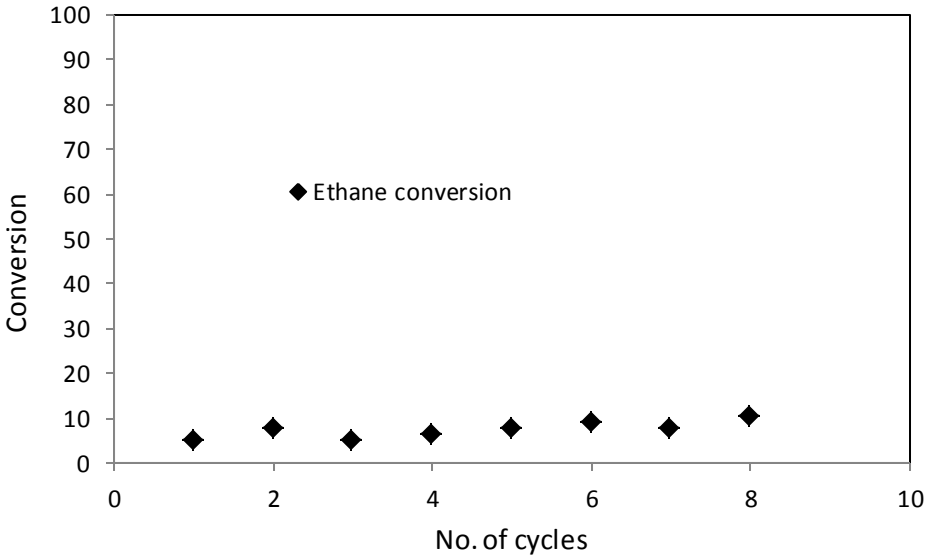


Figure 29: Ethane conversion during multiple cycles in CREC Simulator

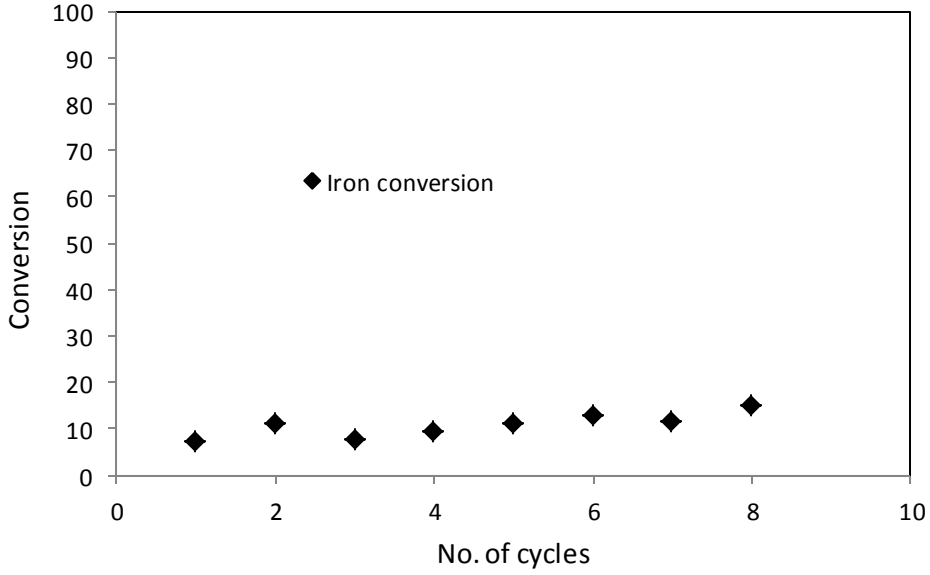


Figure 30: Iron conversion during multiple cycles in CREC Simulator

The conversion of ethane and the oxygen carrier is plotted in Figure 29 and 30 respectively. The ethane conversion is around 8% while the iron oxide conversion is about 11%. The conversion values are low which is predictable since the reaction temperature is low (550 ºC) and the release of the oxygen in iron based oxygen carrier occurs above 600 ºC [55], [56].

The combustion and re-generation reactions occur according to the following suggested reactions:

$$4Fe_2O_3 + CH_4 \rightarrow 8FeO + CO_2 + 2H_2O$$

$$2FeO + \frac{1}{2}O_2 \rightarrow Fe_2O_3$$

### 5.5.2 Ni based oxygen carriers

Following the promising characteristics, the NiO/Ce(1)-$\gamma Al_2O_3$ oxygen carrier was further evaluated in a fluidized CREC Riser Simulator using methane as fuel and air to re-generate the reduced oxygen carrier. In the open literature, there are studies suggested to operate CLC at high temperatures (~ 1200 °C) in order to achieve higher efficiency for power generation [68], [72], [73]. Although performing CLC at high temperature conditions increases the efficiency of power generation, it has other consequences. The most important one is the possibility of NOx formation in the air reactor at elevated reaction temperature [5], [41]. Beside NOx formation, the high temperature operating also increases the possibility of metal sintering and oxygen carrier particles

agglomeration, which eventually leads to drop in the oxygen carrying capacity of the oxygen carrier in CLC process [72]. Because of the above reasons, the oxygen carrier samples were evaluated at a maximum temperature of 750 °C in both the TPR test and in the CLC experiments the temperature was varied temperatures between 550 °C to 650 °C. After each combustion reaction the oxygen carrier was re-generated by following air at 550 °C for 15 minutes. The reaction time was varied from 10 to 60 seconds to study the effect contact time on the conversion. The repeated methane combustion and oxygen carrier re-generation cycles were performed using the same oxygen carrier sample to test the stability of the oxygen carrier over multiple CLC cycles.

Similar to the case with the iron based oxygen carrier, Figure 31 shows a typical the pressure profile of the reactor system during the methane combustion run. The upper curve represents the pressure inside the reactor chamber, while the lower curve shows the pressure profile of the vacuum box. Before fuel injection, the reactor was kept at 14.7 psi while the vacuum box pressure was 3.7 psi. As soon as the fuel was injected, the reactor pressure sharply increased. After that, there is a gradual increase in the reactor pressure as a result of the methane combustion with nickel oxide. Once the pre-specified reaction time was over, the isolation valve between the reactor and the vacuum box was opened immediately which ensured the termination of the reaction given the vacuum box maintained at 250 °C with no oxygen. The abrupt decrease of the reactor pressure confirmed the transformation of the reactor products into the vacuum box.

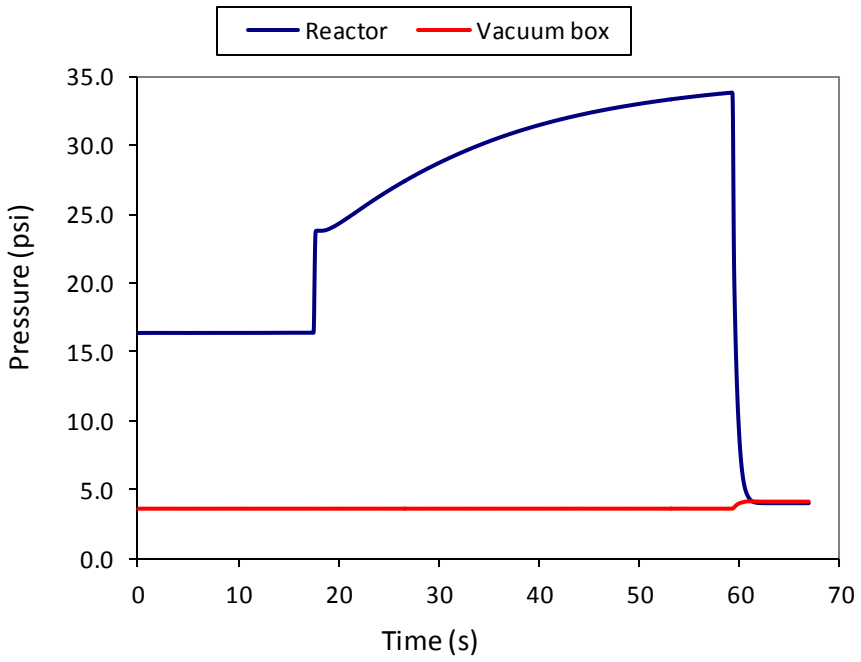


Figure 31: Pressure profile during the combustion process for NiO/Ce(1)-$\gamma Al_2O_3$

The product sample in the vacuum box was analyzed using gas chromatography. The gaseous product mainly contains $CO_2$ and $H_2O$ and trace amount of CO. The very low concentration of CO is due to the complete combustion of methane with NiO [68]. Another reason for the absence of CO in the products might come from the fact that hydrogen and CO very reactive with the nickel oxide as confirmed by the TPR and several previous studies [41], [74]. As a result any traces of CO formed due to incomplete combustion were further converted to $CO_2$ by water-gas shift reaction. Base on the pressure profile and product analysis, on can consider the following reactions during the fluidized bed CLC process with methane [49], [75], [76]:

Fuel combustion

$$CH_4 + 4NiO \rightarrow 4Ni + CO_2 + 2H_2O$$

$H_2 + NiO \rightarrow Ni + H_2O$

$CO + NiO \rightarrow Ni + CO_2$

$CH_4 + NiO \rightarrow Ni + CO + 2H_2$

Reforming

$CH_4 + H_2O \rightarrow CO + 3H_2$

$CH_4 + CO_2 \rightarrow 2CO + 2H_2$

Decomposition

$CH_4 \rightarrow C + 2H_2$

Water-gas shift reaction

$CO + H_2O \rightarrow CO_2 + H_2$

As mentioned before, the reduced oxygen carrier was re-generated by flowing air for 15 minutes to re-oxidize the metal after the combustion process. The following reactions can be proposed to happen during the regeneration process of the oxygen carrier [68], [75]:

$Ni + 1/2O_2 \rightarrow NiO$

$C + O_2 \rightarrow CO_2$

The conversions of methane and nickel oxide are the two important parameters has been assessed from the CLC experiment in the fluidized CREC Riser Simulator. Methane conversion is calculated from the product analysis data considering $CO_2$ is the only carbon containing species in the methane combustion with nickel oxide:

$$X_{CH_4} = \frac{C_{CO_2,out}}{C_{CH_4out} + C_{CO_2,out}} \times 100\,\%$$

where $C_{CH4,out}$ and $C_{CO2,out}$ are the final concentrations of methane and carbon dioxide, respectively, remaining in the reactor after the desired reaction time. Nickel oxide(s) conversion is calculated on the basis of the number of moles of reacted oxygen, the weight of the carrier and the nickel composition of the carrier according to the following equation:

$$X_{NiO} = \frac{4 \times N_{CH_4o} \times X_{CH_4}}{\left( \frac{w \times X_{W,NiO}}{MW_{NiO}} \right)} \times 100\%$$

where $N_{CH4o}$ is the initial number of moles injected into the reactor, $X_{CH4}$ is the conversion of methane, *w* is the mass of oxygen carrier loaded into the reactor, $X_{W,NiO}$ is fraction of nickel oxide present in the oxygen carrier sample and $MW_{NiO}$ is the molecular weight of nickel oxide.

Figure 32 and Figure 33 plots the methane and nickel oxide conversions, respectively during the repeated CLC cycles in fluidized CREC Riser Simulator. It is clear from Figure 12 that the methane conversion increased substantially from about 50% to 88% after modification of the support with cerium oxide. This is due to the improvements in the nickel dispersion and the minimization of nickel aluminate formation which leads to the formation of easily reducible nickel oxide species as shown in TRP/TPO analysis and other characterization results.

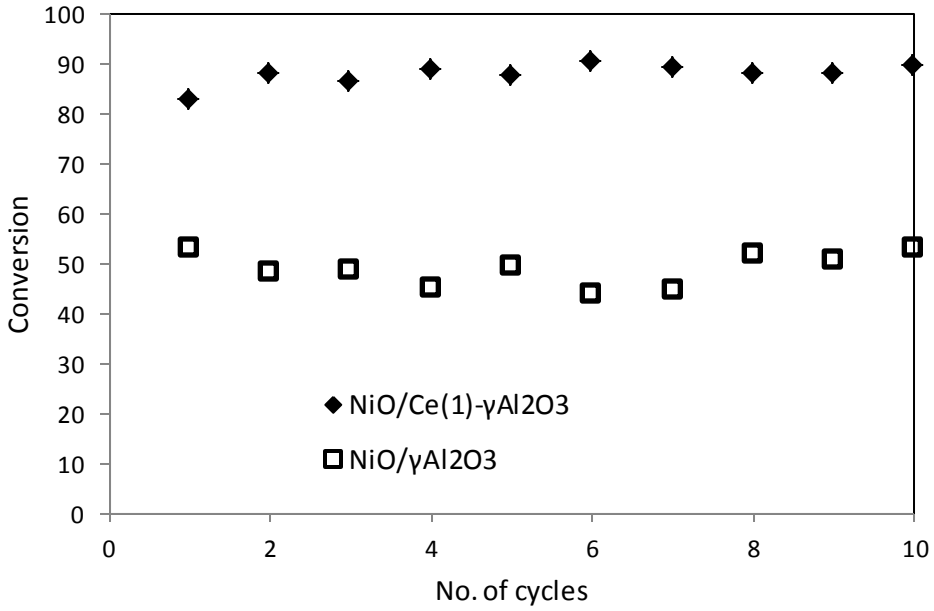


Figure 32: Methane conversion for modified and un-modified oxygen carrier over multiple CLC cycles

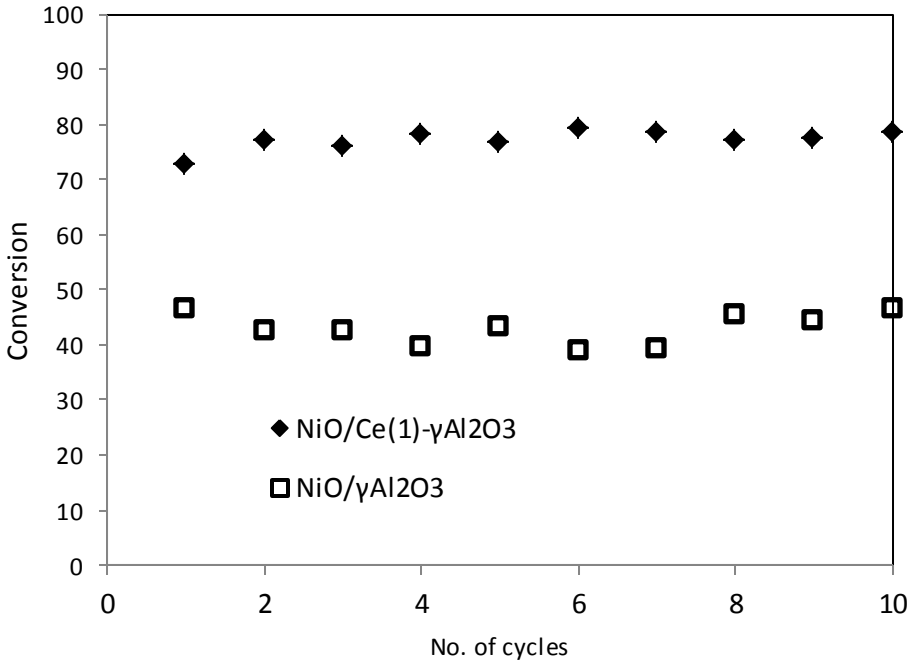


Figure 33: NiO conversion for modified and un-modified oxygen carrier over multiple CLC cycles

The oxygen carrier (NiO) conversion also increased from 44% to 76% after the modification. It is important to mention that the reaction was carried out at 650 °C and the contact time was 40 seconds while the oxygen carrier weight was 0.4 gm. In the case of the unmodified nickel based oxygen carrier ($NiO/\gamma Al_2O_3$) the reduction process was limited by the formation of nickel aluminate that is usually formed when nickel oxide is loaded on alumina.

Figure 34 shows the effects of reaction temperature on the conversion of the oxygen carrier $NiO/Ce(1)\text{-}\gamma Al_2O_3$. The temperature was varied between 550 °C and 650 °C at constant reaction of 40 second. One can see in Figure 34, the oxygen carrier (NiO) conversion with reaction temperature, which is a direct result of the increase in the amount of oxygen released from the oxygen carrier. The conversion of the oxygen carrier was also increased with increasing the reaction time as shown in Figure 35.

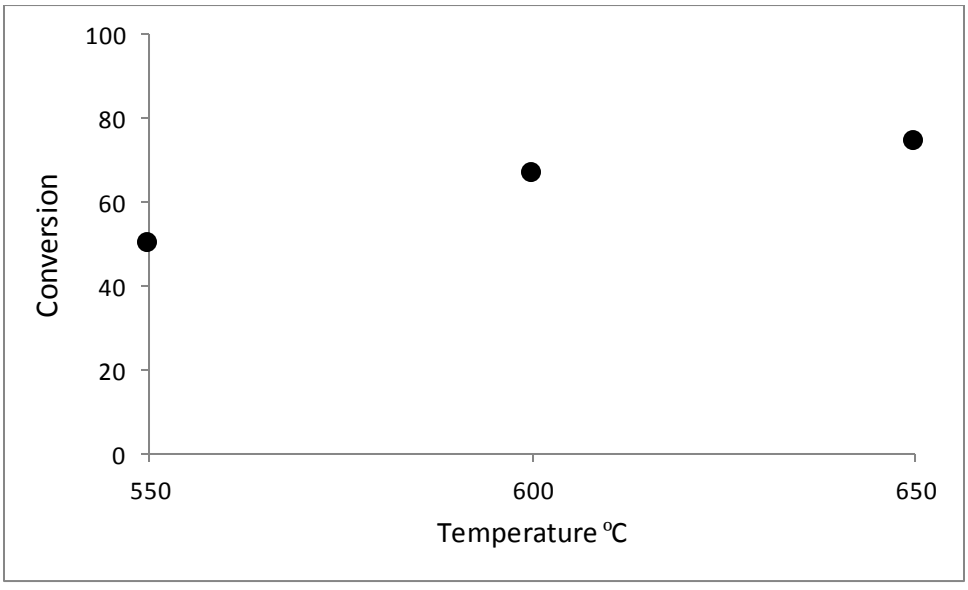


Figure 34: Effect of reaction temperature on NiO conversion

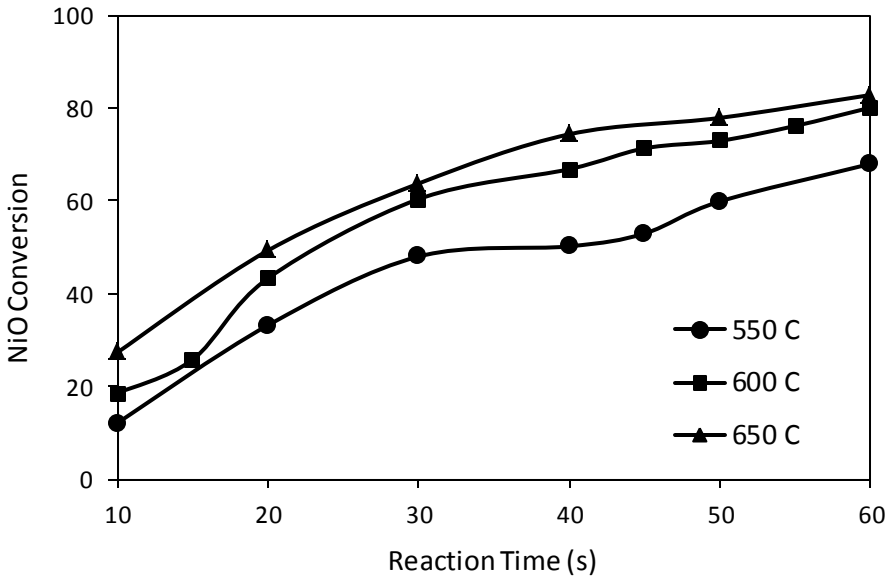


Figure 35: Effect of reaction time on NiO conversion

# CHAPTER 6

# CONCLUSION AND RECOMMENDATIONS

## 6.1 Conclusion

In this investigation fluidizable NiO/Ce-$\gamma Al_2O_3$ and $Fe_2O_3$/Ce-$\gamma Al_2O_3$ oxygen carriers were prepared, characterized and evaluated in a chemical-looping combustion (CLC) cycle of methane/ethane using a fluidized CREC Riser Simulator. Following are the conclusions of this study:

i. The Ce modification improves the thermal stability of support γAl2O3 and helps minimizing the formation of difficult reducing nickel aluminate as revealed by the TPR/TPO analysis. However, excess amount Ce resulted in synergetic interactions between cerium oxide and the metal oxide leading to the increase of the reduction temperatures for the oxygen species.

ii. For iron based oxygen carriers the reduction percentage was low, but it was improved after the modification of the support with 5 wt.% cerium.

iii. NiO on 1 wt % Ce modified $\gamma Al_2O_3$ showed the highest reducibility (94 %). It also reduced below 600 °C, which is highly favorable in CLC application. This sample demonstrates sustained reactivity over the repeated redox cycles. The dispersion of nickel crystal on the Ce modified support remained unchanged with no sign of agglomeration.

iv. TGA and XRD analysis further confirms the stability of the NiO/Ce(1wt%)-$\gamma Al_2O_3$ oxygen carrier with no phase transformation of the support

v. The random nucleation model was found to adequately represent the experimental reduction data, with the parameters being calculated are comparable with that of the literature values.

vi. The NiO/Ce(1wt%)-$\gamma Al_2O_3$ sample display excellent reactivity and stability in repeated CLC cycles in a fluidized bed CREC Riser Simulator using methane as fuel and air to re-generate the reduced oxygen carrier.

vii. The combustion of methane with NiO/Ce(1wt%)-$\gamma Al_2O_3$ mainly give $CO_2$ as combustion product indicating the complete combustion capability of the synthesized oxygen carriers.

viii. The conversion of ethane in reaction with iron based sample $Fe_2O_3$(20)/Ce(1)-$\gamma Al_2O_3$ was low at around 8% as a result of the low reaction temperature relative to iron based oxygen carriers.

ix. Both iron based and nickel based oxygen carriers were stable under multiple CLC cycles using CREC Riser simulator.

## 6.2 Recommendations

Listed below are the recommendations for future work:

i. Evaluation of the iron based samples in CREC Riser simulator using methane for fuel and increasing the reaction temperature beyond 600 °C.

ii. Testing the oxygen carriers in CLC experiments using different types of fuels such as mixture of methane and ethane, liquid fuels, solid fuels etc.

iii. Preparation of oxygen carriers using more than one metal oxide to improve the overall performance of the oxygen carrier.

# References


[1] V. B. and P. M. M. Stocker, T.F., D. Qin, G.-K. Plattner, M. Tignor, S.K. Allen, J. Boschung, A. Nauels, Y. Xia and (eds.), "Climate Change 2013: The Physical Science Basis. Contribution of Working Group I to the Fifth Assessment Report of the Intergovernmental Panel on Climate Change," 2013.

[2] IPCC, "Climate Change 2007 : Synthesis Report," 2007.

[3] S. VijayaVenkataRaman, S. Iniyan, and R. Goic, "A review of climate change, mitigation and adaptation," *Renew. Sustain. Energy Rev.*, vol. 16, no. 1, pp. 878–897, 2012.

[4] J. D. Figueroa, T. Fout, S. Plasynski, H. McIlvried, and R. D. Srivastava, "Advances in CO2 capture technology—The U.S. Department of Energy's Carbon Sequestration Program," *Int. J. Greenh. Gas Control*, vol. 2, no. 1, pp. 9–20, Jan. 2008.

[5] J. Adanez, A. Abad, F. Garcia-Labiano, P. Gayan, and L. F. de Diego, "Progress in Chemical-Looping Combustion and Reforming technologies," *Prog. Energy Combust. Sci.*, vol. 38, no. 2, pp. 215–282, Apr. 2012.

[6] D. Satterthwaite, "Cities' contribution to global warming: notes on the allocation of greenhouse gas emissions," *Environ. Urban.*, vol. 20, no. 2, pp. 539–549, 2008.

[7] J. Fenger, "Air pollution in the last 50 years – From local to global," *Atmos. Environ.*, vol. 43, no. 1, pp. 13–22, Jan. 2009.

[8] I. E. Agency, *World Energy Outlook: China and India Insights*. IEA PUBLICATIONS, 2007.

[9] M. M. Hossain and H. I. de Lasa, "Chemical-looping combustion (CLC) for inherent separations—a review," *Chem. Eng. Sci.*, vol. 63, no. 18, pp. 4433–4451, Sep. 2008.

[10] A. a. Olajire, "CO2 capture and separation technologies for end-of-pipe applications – A review," *Energy*, vol. 35, no. 6, pp. 2610–2628, Jun. 2010.

[11] D. Adams and J. Davison, "Capturing CO2," May 2007.

[12] M. L. Gray, Y. Soong, K. J. Champagne, H. Pennline, J. P. Baltrus, R. W. Stevens Jr, R. Khatri, S. S. C. Chuang, and T. Filburn, "Improved immobilized carbon

dioxide capture sorbents," *Fuel Process. Technol.*, vol. 86, no. 14, pp. 1449–1455, 2005.

[13] J. Davison, P. Freund, and A. Smith, "Putting Carbon Back Into the Ground," 2001.

[14] H. J. Richter and K. F. Knoche, "Reversibility of Combustion Processes," in *Efficiency and Costing: Second Law Analysis of Process*, vol. 235, R. A. Gaggioli, Ed. AMERICAN CHEMICAL SOCIETY, 1983, pp. 71–85.

[15] X. Zhang, W. Han, H. Hong, and H. Jin, "A chemical intercooling gas turbine cycle with chemical-looping combustion," *Energy*, vol. 34, no. 12, pp. 2131–2136, Dec. 2009.

[16] M. Ishida and H. Jin, "A novel chemical-looping combustor without NOx formation," *Ind. Eng. Chem. Res.*, vol. 35, no. 7, pp. 2469–2472, 1996.

[17] J. Adánez and L. De Diego, "Selection of oxygen carriers for chemical-looping combustion," *Energy & Fuels*, no. 3, pp. 371–377, 2004.

[18] P. Cho, T. Mattisson, and A. Lyngfelt, "Comparison of iron-, nickel-, copper-and manganese-based oxygen carriers for chemical-looping combustion," *Fuel*, vol. 83, no. 9, pp. 1215–1225, 2004.

[19] M. Arjmand, H. Leion, T. Mattisson, and A. Lyngfelt, "Investigation of different manganese ores as oxygen carriers in chemical-looping combustion (CLC) for solid fuels," *Appl. Energy*, vol. 113, pp. 1883–1894, Jan. 2014.

[20] A. Cabello, C. Dueso, F. García-Labiano, P. Gayán, A. Abad, L. F. de Diego, and J. Adánez, "Performance of a highly reactive impregnated Fe2O3/Al2O3 oxygen carrier with CH4 and H2S in a 500Wth CLC unit," *Fuel*, vol. 121, pp. 117–125, Apr. 2014.

[21] J.-I. Baek, C. K. Ryu, J. H. Lee, T. H. Eom, J. B. Lee, H.-J. Ryu, J. Ryu, and J. Yi, "The effects of using structurally less-stable raw materials for the support of a spray-dried oxygen carrier with high NiO content," *Fuel*, vol. 102, pp. 106–114, Dec. 2012.

[22] L. F. de Diego, F. García-Labiano, J. Adánez, P. Gayán, A. Abad, B. M. Corbella, and J. María Palacios, "Development of Cu-based oxygen carriers for chemical-looping combustion," *Fuel*, vol. 83, no. 13, pp. 1749–1757, Sep. 2004.

[23] T. A. Brown, F. Scala, S. A. Scott, J. S. Dennis, and P. Salatino, "The attrition behaviour of oxygen-carriers under inert and reacting conditions," *Chem. Eng. Sci.*, vol. 71, pp. 449–467, 2012.

[24] P. Moldenhauer, M. Rydén, T. Mattisson, and A. Lyngfelt, "Chemical-looping combustion and chemical-looping with oxygen uncoupling of kerosene with Mn- and Cu-based oxygen carriers in a circulating fluidized-bed 300W laboratory reactor," *Fuel Process. Technol.*, vol. 104, pp. 378–389, Dec. 2012.

[25] E. Jerndal, T. Mattisson, I. Thijs, F. Snijkers, and A. Lyngfelt, "NiO particles with Ca and Mg based additives produced by spray- drying as oxygen carriers for chemical-looping combustion," *Energy Procedia*, vol. 1, no. 1, pp. 479–486, Feb. 2009.

[26] A. Abad, T. Mattisson, A. Lyngfelt, and M. Johansson, "The use of iron oxide as oxygen carrier in a chemical-looping reactor," *Fuel*, vol. 86, no. 7, pp. 1021–1035, 2007.

[27] M. M. Hossain, D. Lopez, J. Herrera, and H. I. de Lasa, "Nickel on lanthanum-modified γ-Al< sub> 2</sub> O< sub> 3</sub> oxygen carrier for CLC: Reactivity and stability," *Catal. Today*, vol. 143, no. 1, pp. 179–186, 2009.

[28] H. ZHAO, L. LIU, D. XU, C. ZHENG, G. LIU, and L. JIANG, "NiO/NiAl2O4 oxygen carriers prepared by sol-gel for chemical-looping combustion fueled by gas," *J. Fuel Chem. Technol.*, vol. 36, no. 3, pp. 261–266, Jun. 2008.

[29] P. Erri and A. Varma, "Solution combustion synthesized oxygen carriers for chemical looping combustion," *Chem. Eng. Sci.*, vol. 62, no. 18–20, pp. 5682–5687, Sep. 2007.

[30] A. Abad, J. Adánez, F. García-Labiano, L. F. de Diego, and P. Gayán, "Modeling of the chemical-looping combustion of methane using a Cu-based oxygen-carrier," *Combust. Flame*, vol. 157, no. 3, pp. 602–615, 2010.

[31] C. R. Forero, P. Gayán, F. García-Labiano, L. F. de Diego, A. Abad, and J. Adánez, "High temperature behaviour of a CuO/γAl2O3 oxygen carrier for chemical-looping combustion," *Int. J. Greenh. Gas Control*, vol. 5, no. 4, pp. 659–667, Jul. 2011.

[32] I. M. Dahl, E. Bakken, Y. Larring, A. I. Spjelkavik, S. F. Håkonsen, and R. Blom, "On the development of novel reactor concepts for chemical looping combustion," *Energy Procedia*, vol. 1, no. 1, pp. 1513–1519, 2009.

[33] S. Y. Chuang, J. S. Dennis, A. N. Hayhurst, and S. A. Scott, "Development and performance of Cu-based oxygen carriers for chemical-looping combustion," *Combust. Flame*, vol. 154, no. 1, pp. 109–121, 2008.

[34] M. K. Chandel, a. Hoteit, and a. Delebarre, "Experimental investigation of some metal oxides for chemical looping combustion in a fluidized bed reactor," *Fuel*, vol. 88, no. 5, pp. 898–908, May 2009.

[35] A. Abad, I. Adánez-Rubio, P. Gayán, F. García-Labiano, L. F. de Diego, and J. Adánez, "Demonstration of chemical-looping with oxygen uncoupling (CLOU) process in a 1.5kWth continuously operating unit using a Cu-based oxygen-carrier," *Int. J. Greenh. Gas Control*, vol. 6, pp. 189–200, Jan. 2012.

[36] B. M. Corbella and J. M. Palacios, "Titania-supported iron oxide as oxygen carrier for chemical-looping combustion of methane," *Fuel*, vol. 86, no. 1, pp. 113–122, 2007.

[37] Q. Tan, W. Qin, Q. Chen, C. Dong, W. Li, and Y. Yang, "Synergetic effect of ZrO2 on the oxidation–reduction reaction of Fe2O3 during chemical looping combustion," *Appl. Surf. Sci.*, vol. 258, no. 24, pp. 10022–10027, Oct. 2012.

[38] P. Gayán, C. Dueso, A. Abad, J. Adanez, L. F. de Diego, and F. García-Labiano, "NiO/Al2O3 oxygen carriers for chemical-looping combustion prepared by impregnation and deposition–precipitation methods," *Fuel*, vol. 88, no. 6, pp. 1016–1023, Jun. 2009.

[39] C. Dueso, A. Abad, F. García-Labiano, L. F. de Diego, P. Gayán, J. Adánez, and A. Lyngfelt, "Reactivity of a NiO/Al2O3 oxygen carrier prepared by impregnation for chemical-looping combustion," *Fuel*, vol. 89, no. 11, pp. 3399–3409, Nov. 2010.

[40] M. M. Hossain, M. R. Quddus, and H. I. de Lasa, "Reduction Kinetics of La Modified NiO/La-γAl2O3 Oxygen Carrier for Chemical-Looping Combustion," *Ind. Eng. Chem. Res.*, vol. 49, no. 21, pp. 11009–11017, Jun. 2010.

[41] M. R. Quddus, M. M. Hossain, and H. I. de Lasa, "Ni based oxygen carrier over γ-Al2O3 for chemical looping combustion: Effect of preparation method on metal support interaction," *Catal. Today*, vol. 210, pp. 124–134, Jul. 2013.

[42] J.-I. Baek, J. Ryu, J. B. Lee, T.-H. Eom, K.-S. Kim, S.-R. Yang, and C. K. Ryu, "Highly attrition resistant oxygen carrier for chemical looping combustion," *Energy Procedia*, vol. 4, pp. 349–355, Jan. 2011.

[43] J. E. Readman, A. Olafsen, J. B. Smith, and R. Blom, "Chemical Looping Combustion Using NiO/NiAl 2 O 4 : Mechanisms and Kinetics of Reduction−Oxidation (Red-Ox) Reactions from In Situ Powder X-ray Diffraction and Thermogravimetry Experiments," *Energy & Fuels*, vol. 20, no. 4, pp. 1382–1387, Jul. 2006.

[44] M. Ishida, M. Yamamoto, and T. Ohba, "Experimental results of chemical-looping combustion with NiO/NiAl2O4 particle circulation at 1200 °C," *Energy Convers. Manag.*, vol. 43, no. 9–12, pp. 1469–1478, Jun. 2002.

[45] M. M. Hossain and H. I. de Lasa, "Reduction and oxidation kinetics of Co–Ni/Al2O3 oxygen carrier involved in a chemical-looping combustion cycles," *Chem. Eng. Sci.*, vol. 65, no. 1, pp. 98–106, Jan. 2010.

[46] K. E. Sedor, M. M. Hossain, and H. I. de Lasa, "Reactivity and stability of Ni/Al2O3 oxygen carrier for chemical-looping combustion (CLC)," *Chem. Eng. Sci.*, vol. 63, no. 11, pp. 2994–3007, Jun. 2008.

[47] C. Linderholm, A. Abad, T. Mattisson, and A. Lyngfelt, "160h of chemical-looping combustion in a 10kW reactor system with a NiO-based oxygen carrier," *Int. J. Greenh. Gas Control*, vol. 2, no. 4, pp. 520–530, Oct. 2008.

[48] Z. Deng, R. Xiao, B. Jin, and Q. Song, "Numerical simulation of chemical looping combustion process with CaSO4 oxygen carrier," *Int. J. Greenh. Gas Control*, vol. 3, no. 4, pp. 368–375, Jul. 2009.

[49] A. Bischi, Ø. Langørgen, I. Saanum, J. Bakken, M. Seljeskog, M. Bysveen, J.-X. Morin, and O. Bolland, "Design study of a 150kWth double loop circulating fluidized bed reactor system for chemical looping combustion with focus on industrial applicability and pressurization," *Int. J. Greenh. Gas Control*, vol. 5, no. 3, pp. 467–474, May 2011.

[50] O. Levenspiel, *Chemical reaction engineering*, vol. 2. Wiley New York etc., 1972.

[51] H. Kruggel-Emden, F. Stepanek, and A. Munjiza, "A comparative study of reaction models applied for chemical looping combustion," *Chem. Eng. Res. Des.*, vol. 89, no. 12, pp. 2714–2727, 2011.

[52] J. Szekely, C. I. Lin, and H. Y. Sohn, "A structural model for gas—solid reactions with a moving boundary—V an experimental study of the reduction of porous nickel-oxide pellets with hydrogen," *Chem. Eng. Sci.*, vol. 28, no. 11, pp. 1975–1989, Nov. 1973.

[53] C. Georgakis, C. W. Chang, and J. Szekely, "A changing grain size model for gas—solid reactions," *Chem. Eng. Sci.*, vol. 34, no. 8, pp. 1072–1075, Jan. 1979.

[54] H. I. De Lasa, "Riser simulator," U.S. Patent No. 5,102,62807-Apr-1992.

[55] J. Wang, M. Shen, J. Wang, M. Cui, J. Gao, J. Ma, and S. Liu, "Preparation of FexCe1-xOy solid solution and its application in Pd-only three-way catalysts," *J. Environ. Sci.*, vol. 24, no. 4, pp. 757–764, Apr. 2012.

[56] P. Webb Orr, Clyde., Micromeritics Instrument Corporation.,, *Analytical methods in fine particle technology*. Norcross, Ga.: Micromeritics Instrument Corp., 1997.

[57] K. Xavier, R. Sreekala, and K. Rashid, "Doping effects of cerium oxide on Ni/Al 2 O 3 catalysts for methanation," *Catal. today*, vol. 49, 1999.

[58] Q. Zhuang and L. Chang, "Promoting effect of cerium oxide in supported nickel catalyst for hydrocarbon steam-reforming," *Appl. Catal.*, vol. 70, no. 1, pp. 1–8, 1991.

[59] J. P. Bortolozzi, L. B. Gutierrez, and M. a. Ulla, "Efficient structured catalysts for ethylene production through the ODE reaction: Ni and Ni–Ce on ceramic foams," *Catal. Commun.*, vol. 43, no. 3, pp. 197–201, Jan. 2014.

[60] S. J. Tauster, "Strong metal-support interactions," *Acc. Chem. Res.*, vol. 20, no. 11, pp. 389–394, 1987.

[61] Y. Chung, G. Xiong, and C. Kao, "Mechanism of strong metal-support interaction in NiTiO2," *J. Catal.*, vol. 243, pp. 237–243, 1984.

[62] S. Bernal, J. J. Calvino, M. A. Cauqui, J. M. Gatica, C. López Cartes, J. A. Pérez Omil, and J. M. Pintado, "Some contributions of electron microscopy to the characterisation of the strong metal–support interaction effect," *Catal. Today*, vol. 77, no. 4, pp. 385–406, Jan. 2003.

[63] G. Wrobel, M. Sohier, and A. D'Huysser, "Hydrogenation catalysts based on nickel and rare earth oxides: Part II: XRD, electron microscopy and XPS studies of the cerium-nickel-oxygen-hydrogen system," *Appl. Catal. A ...*, vol. 101, no. 402, pp. 73–93, 1993.

[64] H. L. Rotgerink and J. Slaa, "Studies on the promotion of nickel—alumina coprecipitated catalysts: III. Cerium oxide," *Appl. Catal.*, vol. 45, pp. 281–290, 1988.

[65] T. Y. Kim, S. M. Kim, W. S. Lee, and S. I. Woo, "Effect and behavior of cerium oxide in Ni/γ-Al2O3 catalysts on autothermal reforming of methane: CeAlO3 formation and its role on activity," *Int. J. Hydrogen Energy*, vol. 38, no. 14, pp. 6027–6032, May 2013.

[66] T. Osawa, Y. Nakai, A. Mouri, and I.-Y. S. Lee, "Studies of the preparation method of ceria-promoted nickel catalyst for carbon dioxide reforming of methane," *Appl. Catal. A Gen.*, no. 00, pp. 2–8, Aug. 2013.

[67] H. Liu, H. Wang, J. Shen, Y. Sun, and Z. Liu, "Promotion effect of cerium and lanthanum oxides on Ni/SBA-15 catalyst for ammonia decomposition," *Catal. Today*, vol. 131, no. 1–4, pp. 444–449, Feb. 2008.

[68] M. M. Hossain and H. I. de Lasa, "Reactivity and stability of Co- Ni/Al2O3 oxygen carrier in multicycle CLC," *AIChE J.*, vol. 53, no. 7, pp. 1817–1829, 2007.

[69] K. E. Sedor, M. M. Hossain, and H. I. de Lasa, "Reduction kinetics of a fluidizable nickel–alumina oxygen carrier for chemical-looping combustion," *Can. J. Chem. Eng.*, vol. 86, no. 3, pp. 323–334, Jun. 2008.

[70] S. R. Son and S. D. Kim, "Chemical-looping combustion with NiO and Fe2O3 in a thermobalance and circulating fluidized bed reactor with double loops," *Ind. Eng. Chem. Res.*, vol. 45, no. 8, pp. 2689–2696, 2006.

[71] B. Moghtaderi and H. Song, "Reduction properties of physically mixed metallic oxide oxygen carriers in chemical looping combustion," *Energy & Fuels*, vol. 24, no. 10, pp. 5359–5368, 2010.

[72] J. Wolf, M. Anheden, and J. Yan, "Comparison of nickel-and iron-based oxygen carriers in chemical looping combustion for CO< sub> 2</sub> capture in power generation," *Fuel*, vol. 84, no. 7, pp. 993–1006, 2005.

[73] J. Wolf and J. Yan, "Parametric study of chemical looping combustion for tri-generation of hydrogen, heat, and electrical power with CO2 capture," *Int. J. Energy Res.*, vol. 29, no. 8, pp. 739–753, Jun. 2005.

[74] M. Ortiz, L. F. de Diego, A. Abad, F. García-Labiano, P. Gayán, and J. Adánez, "Catalytic activity of Ni-based oxygen-carriers for steam methane reforming in chemical-looping processes," *Energy & Fuels*, vol. 26, no. 2, pp. 791–800, 2012.

[75] P. Gayán, L. F. de Diego, F. García-Labiano, J. Adánez, A. Abad, and C. Dueso, "Effect of support on reactivity and selectivity of Ni-based oxygen carriers for chemical-looping combustion," *Fuel*, vol. 87, no. 12, pp. 2641–2650, Sep. 2008.

[76] T. Mattisson, E. Jerndal, C. Linderholm, and A. Lyngfelt, "Reactivity of a spray-dried NiO/NiAl2O4 oxygen carrier for chemical-looping combustion," *Chem. Eng. Sci.*, vol. 66, no. 20, pp. 4636–4644, Oct. 2011.

]

# Vitae


Name Shamseldin Awad Hagahmed Mohamed

Nationality Sudanese

Date of Birth 7/25/1988

Email shamseldin.mohamed@hotmail.com

Address Khartoum, Sudan


Academic Background :

M.S. in Chemical Engineering 2014
King Fahd University of Petroleum and Minerals
*Dhahran, Saudi Arabia*

B.S. in Chemical Engineering 2010
University of Khartoum
*Khartoum, Sudan*

Conferences:

**Shamseldin Mohamed**, ShaikhRazzak, Mohammad R. Quddus, Hugo I. de Lasa and Mohammad M. Hossain, **"NiO/Ce-γ$Al_2O_3$ Oxygen Carrier for Chemical-Looping Combustion: Reactivity and Stability"**, AIChE Annual Meeting, 2013.

**Shamseldin Mohamed,** Mohammad M. Hossain, ShaikhRazzak, **"$Fe_2O_3$/Ce-γ$Al_2O_3$ Oxygen Carrier for Chemical Looping Combustion"**
23rd Canadian Symposium on Catalysis, Alberta, Canada.